Astronomy & Astrophysics manuscript no. article
February 16, 2016
© ESO 2016

arXiv:1602.04622v1 [astro-ph.EP] 15 Feb 2016

The SOPHIE search for northern extrasolar planets⋆

X. Detection and characterization of giant planets by the dozen

G. Hébrard[1,2], L. Arnold[2], T. Forveille[3], A. C. M. Correia[4,5], J. Laskar[5], X. Bonfils[3], I. Boisse[6], R. F. Díaz[7], J. Hagelberg[8], J. Sahlmann[9], N. C. Santos[10,11], N. Astudillo-Defru[3,7], S. Borgniet[3], F. Bouchy[6], V. Bourrier[7,1], B. Courcol[6], X. Delfosse[3], M. Deleuil[6], O. Demangeon[6], D. Ehrenreich[7], J. Gregorio[12], N. Jovanovic[13,14], O. Labrevoir[15], A.-M. Lagrange[3], C. Lovis[7], J. Lozi[13], C. Moutou[6,16], G. Montagnier[1,2], F. Pepe[7], J. Rey[7], A. Santerne[10], D. Ségransan[7], S. Udry[7], M. Vanhuysse[17], A. Vigan[6], P. A. Wilson[1]

[1] Institut d'Astrophysique de Paris, UMR7095 CNRS, Université Pierre & Marie Curie, 98bis boulevard Arago, 75014 Paris, France
e-mail: hebrard@iap.fr
[2] Observatoire de Haute-Provence, CNRS, Université d'Aix-Marseille, 04870 Saint-Michel-l'Observatoire, France
[3] Université J. Fourier (Grenoble 1)/CNRS, Laboratoire d'Astrophysique de Grenoble (LAOG, UMR5571), France
[4] CIDMA, Departamento de Física, Universidade de Aveiro, Campus de Santiago, 3810-193 Aveiro, Portugal
[5] ASD/IMCCE, CNRS-UMR8028, Observatoire de Paris, PSL, UPMC, 77 Avenue Denfert-Rochereau, 75014 Paris, France
[6] Aix Marseille Université, CNRS, LAM (Laboratoire d'Astrophysique de Marseille) UMR 7326, 13388 Marseille, France
[7] Observatoire de Genève, Université de Genève, 51 Chemin des Maillettes, 1290 Sauverny, Switzerland
[8] Institute for Astronomy, University of Hawaii, 2680 Woodlawn Drive, Honolulu, HI 96822, USA
[9] European Space Agency, European Space Astronomy Centre, P.O. Box 78, Villanueva de la Canada, 28691 Madrid, Spain
[10] Instituto de Astrofísica e Ciências do Espaço, Universidade do Porto, CAUP, Rua das Estrelas, 4150-762 Porto, Portugal
[11] Departamento de Física e Astronomia, Faculdade de Ciências, Universidade do Porto, Rua Campo Alegre, 4169-007 Porto, Portugal
[12] Atalaia Group, CROW-Observatory Portalegre, Portugal
[13] National Astronomical Observatory of Japan, Subaru Telescope, 650 North A'Ohoku Place, Hilo, HI, 96720, USA
[14] Department of Physics and Astronomy, Macquarie University, NSW 2109, Australia
[15] Centre d'Astronomie, Plateau du Moulin à Vent, 04870 Saint-Michel-l'Observatoire, France
[16] Canada France Hawaii Telescope Corporation, Kamuela, HI 96743, USA
[17] Oversky, 47 Allée des Palanques, 33127 Saint-Jean-d'Illac, France

Received TBC; accepted TBC

ABSTRACT

We present new radial velocity measurements of eight stars secured with the spectrograph SOPHIE at the 193-cm telescope of the Haute-Provence Observatory allowing the detection and characterization of new giant extrasolar planets. The host stars are dwarfs of spectral types between F5 and K0 and magnitudes between 6.7 and 9.6; the planets have minimum masses $M_{\rm p} \sin i$ between 0.4 to 3.8 $M_{\rm Jup}$ and orbital periods of several days to several months. The data allow only single planets to be discovered around the first six stars (HD 143105, HIP 109600, HD 35759, HIP 109384, HD 220842, and HD 12484), but one of them shows the signature of an additional substellar companion in the system. The seventh star, HIP 65407, allows the discovery of two giant planets, just outside the 12:5 resonance in weak mutual interaction. The last star, HD 141399, was already known to host a four-planetary system; our additional data and analyses allow new constraints to be put on it. We present Keplerian orbits of all systems, together with dynamical analyses of the two multi-planetary systems. HD 143105 is one of the brightest stars known to host a hot Jupiter, which could allow numerous follow-up studies to be conducted despite this is not a transiting system. The giant planets HIP 109600b, HIP 109384b, and HD 141399c are located in the habitable zone of their host star.

Key words. planetary systems – techniques: radial velocities – stars: individual: HD 143105, HIP 109600, HD 35759, HIP 109384, HD 220842, HD 12484, HIP 65407, HD 141399

1. Introduction

Since its installation in late 2006 at the 193-cm telescope of the Haute-Provence Observatory (OHP), the spectrograph SOPHIE is used among other programs to perform a volume-limited survey of giant extrasolar planets (Bouchy et al. 2009). The goal of that survey is to improve the statistics on the exoplanet parameters and their hosting stars by increasing the number of known Jupiter-mass planets, as well as identify particular cases allowing interesting follow-up studies, e.g. on dynamics for multi-planetary systems, or on structure characterization if they turn out to transit their host star. Indeed, numerous questions concerning giant planets remain open, first of all their formation processes which could operate through core-accretion (e.g. Mordasini et al. 2009; Guilera et al. 2010) or disk-instability (e.g. Cai et al. 2010; Boss 2011) models. Their subsequent

Send offprint requests to: G. Hébrard (hebrard@iap.fr)

⋆ Based on observations collected with the SOPHIE spectrograph on the 1.93-m telescope at Observatoire de Haute-Provence (CNRS), France, by the SOPHIE Consortium (programs 07A.PNP.CONS to 15A.PNP.CONS). The full version of the SOPHIE measurements (Table 1) is only available in electronic form at the CDS via anonymous ftp to cdsarc.u-strasbg.fr (130.79.128.5) or via http://cdsweb.u-strasbg.fr/cgi-bin/qcat?J/A+A/TBC.

evolution is subject to debates as well, concerning for example their migration processes (e.g. Lin et al. 1996; Levison et al. 2006; Carter-Bond et al. 2012) or the existence of a population of inflated close-in planets, likely related to interactions with their host stars, e.g. though tides or irradiation (e.g. Baraffe et al. 2014). The physics of their internal structures (e.g. Liu et al. 2015) and atmospheres (e.g. Sing et al. 2016) are also far to be fully understood. Thus, detecting and characterizing new giant planets provide constraints on the models of their formation and evolution, and allows the exploration of the diversity of planetary systems to be pursued.

Among the ∼ 2000 exoplanets known so far according the Exoplanet Encyclopaedia[1], only about 1100 have a mass measurement, most of them measured from radial velocities. Less than 700 have a mass measured with an accuracy better than ±30 %, and less than 280 have known both mass and radius (Han et al. 2014)[2]. Accurate radial velocity measurements remain an efficient and powerful technique for research and characterization of exoplanetary systems. By comparison to transiting surveys, they are particularly powerful to detect multi-planetary systems and to construct the orbital periods distribution on its longer part. They also provide the planetary masses distribution, allowing super-Earths, giant planets, and brown dwarfs populations to be distinguished and studied.

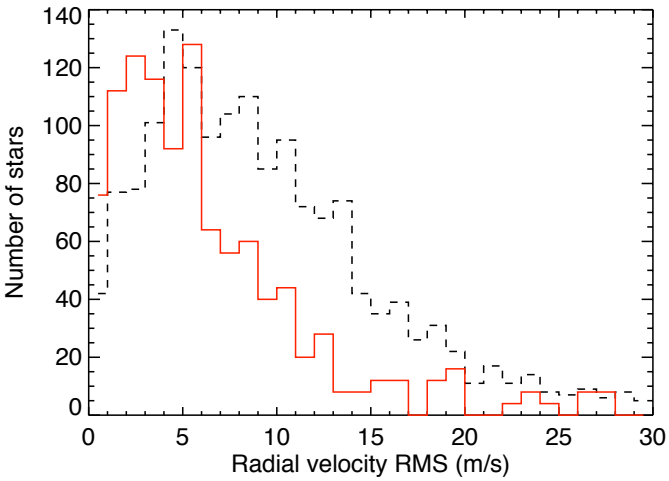

Fig. 1. Histogram of the radial velocity dispersions for 1900 stars observed with SOPHIE since 2006 as part of the giant planets survey (dashed, black). The typical accuracy is of the order of ±7 m/s. The histogram plotted in solid, red line selects only the measurements secured after the SOPHIE improvement done in June 2011; it shows an improvement of the radial velocity accuracy at a level of ±3.5 m/s. To allow a better comparison between both histograms, the *y*-scale of the red histogram has been multiplied by a factor four.

In its current version, the catalog of the SOPHIE survey for giant planets includes 2300 dwarf stars at distance < 60 pc and with $B - V$ between 0.35 and 1.0. Most of them (about 1900) have already been observed with SOPHIE. Figure 1 shows histograms of the radial velocities dispersion of all the stars with at least two SOPHIE measurements. Since its upgrade in June 2011, the typical accuracy of that program was reduced from ±7 m/s down to ±3.5 m/s. The main reason for that amelioration is the SOPHIE fiber-link scrambling properties improvement due to the implementation of pieces of octagonal-section fibers (Bouchy et al. 2013). Such accuracy allows Jupiter-mass planets to be detected on periods up to several years, or Saturn-mass planets on periods up to several months.

That SOPHIE survey has already allowed the detection and characterization of several planets (Da Silva et al. 2008; Santos et al. 2008; Bouchy et al. 2009; Hébrard et al. 2010; Boisse et al. 2010; Moutou et al. 2014; Díaz et al. 2016a) and of more massive companions in the planet-brown dwarf boundary (Díaz et al. 2012; Wilson et al. 2016). Here we present the discovery of six new, single planets in orbit around the stars HD 143105, HIP 109600, HD 35759, HIP 109384, HD 220842, and HD 12484, and of a two-planet system around HIP 65407. We also present new measurements and analyses of the multi-planetary system orbiting HD 141399, previously announced by Vogt et al. (2014) while we were independently monitoring it with SOPHIE.

The SOPHIE observations and data reduction are presented in Sect. 2. We determine the parameters of the host stars in Sect. 3, then derive and discuss the planetary systems properties in Sects. 4 and 5 for single and multi-planetary systems, respectively, before concluding in Sect. 6.

Table 1. Radial velocities (barycentric referential) and bisector span measured with SOPHIE (full table available electronically).

BJD_{UTC} -2 400 000	RV ($km\,s^{-1}$)	$\pm1\,\sigma$ ($km\,s^{-1}$)	Bis ($km\,s^{-1}$)	star	instrument
54366.3748	-70.117	0.006	-0.001	HIP 109600	SOPHIE
55402.6067	-69.929	0.007	0.004	HIP 109600	SOPHIE
55429.5443	-69.955	0.007	0.004	HIP 109600	SOPHIE
55431.4808	-69.974	0.007	0.011	HIP 109600	SOPHIE
...	...	...	...	...	...
...	...	...	...	...	...
56941.2460	-21.541	0.005	-0.033	HD 141399	SOPHIE+
56942.2807	-21.556	0.004	-0.040	HD 141399	SOPHIE+
57088.6956	-21.596	0.003	-0.025	HD 141399	SOPHIE+
57115.5526	-21.602	0.004	-0.029	HD 141399	SOPHIE+

2. SOPHIE spectroscopy and radial velocities

We observed the eight stars with SOPHIE at the OHP 1.93-m telescope. SOPHIE is a cross-dispersed, environmentally stabilized echelle spectrograph dedicated to high-precision radial velocity measurements (Perruchot et al. 2008; Bouchy et al. 2009). Observations were secured in fast reading mode of the detector and *high-resolution* mode of the spectrograph, allowing the resolution power $\lambda/\Delta\lambda = 75000$ to be reached. Depending of the star, the spectra were obtained over timespans of two to eight years. Their typical exposure times are of a few minutes, in order to reach a signal-to-noise ratios per pixel at 550 nm around 50. The total dataset presented here represents nearly 600 exposures for a total integration time exceeding 60 hours on the sky. For all the exposures the first optical fiber aperture was used for starlight whereas the second one was put on the sky to evaluate the sky background pollution, especially from Moonlight. Wavelength calibrations were made at the beginning and the end of each observing night, and with a ∼ 2-hour frequency during the nights. This allows the drift of the instrument to be interpolated at the time of each exposure. Four stars were observed both before

[1] http://exoplanet.eu.
[2] http://exoplanets.org.

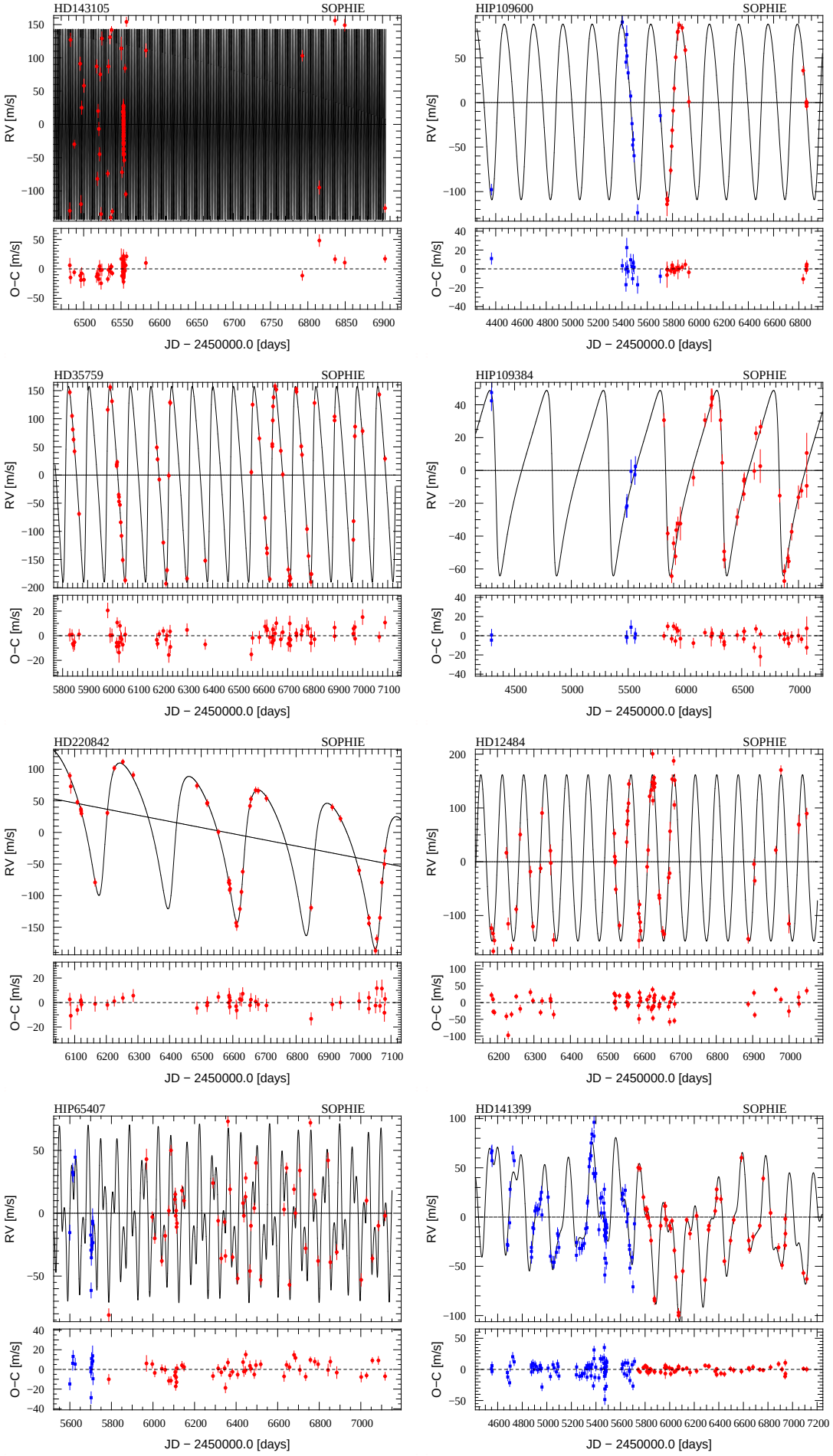

Fig. 2. Radial velocity SOPHIE measurements of the eight stars as a function of time (before/after the June-2011 upgrade are plotted in blue/red), and Keplerian fits. The orbital parameters corresponding to the Keplerian fits are reported in Tables 3 and 4. On each panel, the residuals with 1-σ error bars are plotted below the fit.

and after the SOPHIE upgrade of June 2011 (Sect. 1; Bouchy et al. 2013). As the upgrade introduces significant differences, we considered for each of them two distinct datasets, namely SOPHIE and SOPHIE+, depending whether the data were acquired before or after the upgrade, respectively. The four remaining stars were only observed after the upgrade (SOPHIE+ only).

We used the SOPHIE pipeline (Bouchy et al. 2009) to extract the spectra from the detector images, cross-correlate them with numerical masks which produced clear cross-correlation functions (CCFs), then fit the CCFs by Gaussians to get the radial velocities (Baranne et al. 1996; Pepe et al. 2002). The bisector spans of each CCF were also computed following Queloz et al. (2001). All the 39 SOPHIE spectral orders (covering the wavelength range 3872 Å – 6943 Å) were used for the cross-correlations. The spectra significantly polluted by sky background (in particular Moonlight) were corrected following the method described e.g. by Bonomo et al. (2010). Each exposure was then corrected from the interpolated drift of the instrument. In the case of the SOPHIE+ data, we also applied the "RV constant master" correction presented by Courcol et al. (2015) which takes into account for small additional instrumental drifts.

The derived radial velocities and bisector spans are reported in Table 1. Typical uncertainties are between 3 and 10 m/s depending on the stars properties and actual signal-to-noise of the spectra. This includes photon noise and wavelength calibration uncertainty, the latest being estimated to the order of 2 m/s for each exposure. For the exposures obtained before the June 2011 upgrade, we also quadratically added a 5-m/s additional uncertainty due to poor scrambling properties at that time (Bouchy et al. 2013). The final uncertainties do not include any "jitter" due to stellar activity. The uncertainties reported here are significantly larger than those obtained with SOPHIE+ by Courcol et al. (2015) on stars of similar magnitudes and spectral types to detect low-mass planets. This is due to three main reasons. Firstly, the exposure times and obtained signal-to-noise ratios are smaller here, so the radial velocity uncertainty due photon noise is larger. Secondly, as the exposure times are shorter, the short-term stellar intrinsic variations are less efficaciously averaged out. Finally, the SOPHIE observations of Courcol et al. (2015) are done with simultaneous wavelength calibration in the second entrance aperture, which is not the case here. This illustrates the different strategies adopted with a given instrument to reach distinct goals. The present program aiming at detecting giant planets, it could be done at lower accuracy. In addition, it does not need perfect weather conditions and could continue even in cases of thin clouds in the sky, large seeing, or significant sky background pollution due to Moonlight or even twilight.

The SOPHIE radial velocities of the eight stars are plotted in Fig. 2 as a function of time. They all show variations well over the expected dispersion due to the measurement accuracy and the possible stellar jitter. The bisectors of the CCFs (Table 1) are stable for each object; they show dispersions well below that of the radial velocities variations. An anticorrelation between the bisector and the radial velocity is usually the signature of radial velocity variations induced by stellar activity (see, e.g., Queloz et al. 2001; Boisse et al. 2009). Lomb-Scargle periodograms of the bisectors do not show any significant feature either. Similarly, other indicators linked to stellar activity, including CCF widths or Ca II emission index $\log R'_{\rm HK}$, do not show any significant peaks in their periodograms. All of this indicates the radial velocity variations are mainly due to Doppler shifts of the stellar lines rather than stellar profile variations. This leads to concluding that reflex motions due to companion(s) are the likely causes of the stellar radial velocity variations. The amplitudes of the variations put the companions in the planet-mass regime.

3. Properties of the eight planet-host stars

Table 2 summarizes the stellar parameters of the eight planet-host stars. Magnitudes, $B-V$, and parallaxes are from Hipparcos (Perryman et al. 1997). For each star we constructed an averaged spectrum using all the SOPHIE spectra unaffected by Moon pollution, and we performed spectral analyses from them. We used the method presented in Santos et al. (2004) and Sousa et al. (2008) to derive the effective temperatures $T_{\rm eff}$, the surface gravities $\log g$, and the metallicities [Fe/H]. The metallicities computed using the CCF calibration presented by Boisse et al. (2010) agree with the above ones, but we did not adopt these values as they are less accurate (typically ±0.09 dex) than those obtained from stellar spectroscopic analysis. Using those derived spectroscopic parameters as input, stellar masses were derived from the calibration of Torres et al. (2010) with a correction following Santos et al. (2013). Errors were computed from 10,000 random values of the stellar parameters within their error bars and assuming Gaussian distributions. We derived the projected rotational velocities $v \sin i_\star$ and their uncertainties from the parameters of the CCF using the calibration of Boisse et al. (2010).

The eight planet hosts are dwarf stars of spectral types between F5 and K0. Three stars are metal-poor (HIP 109600, HIP 109384, and HD 220842) and three are metal-rich (HD 143105, HIP 65407, and HD 141399), the two remaining ones having Solar metallicities. They show standard, slow rotations with $v \sin i_\star$ of the order of 2 to 4 km/s, with the two exceptions of HD 143105 and HD 12484 showing faster rotations with $v \sin i_\star$ of the order of 8 to 9 km/s.

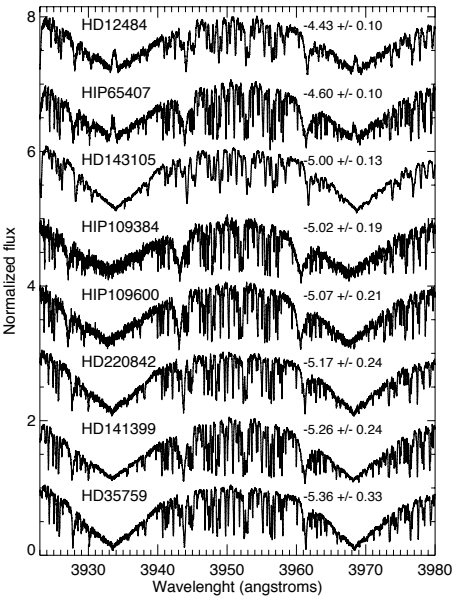

Fig. 3. H and K Ca II lines of the eight planet-host stars on the averaged SOPHIE spectra. The stars are sorted by increasing activity from bottom to top, with the $\log R'_{\rm HK}$ values overplotted on the right. The flux of HD 35759 is the correct one; each star plotted above is successively shifted by 1 on the y-scale for visibility reasons. Only HD 12484 and HIP 65407 show visually significant chromospheric emissions.

Table 2. Adopted stellar parameters for the eight host stars (see Sect. 3).

Parameter	HD 143105	HIP 109600	HD 35759	HIP 109384	HD 220842	HD 12484	HIP 65407	HD 141399
m_v	6.75 ± 0.01	9.16 ± 0.02	7.74 ± 0.01	9.63 ± 0.02	7.99 ± 0.01	8.17 ± 0.01	9.42 ± 0.02	7.20 ± 0.02
Spectral type†	F5	G5	G0	G5	F8	F8	K0	K0
$B - V$	0.52 ± 0.01	0.75 ± 0.03	0.59 ± 0.01	0.79 ± 0.04	0.58 ± 0.02	0.66 ± 0.02	0.78 ± 0.04	0.73 ± 0.04
Parallax [mas]	20.55 ± 0.34	17.12 ± 0.93	13.83 ± 0.76	17.84 ± 0.85	16.03 ± 0.73	19.61 ± 0.97	16.74 ± 1.28	27.65 ± 0.37
Distance [pc]	48.7 ± 0.8	58.6 ± 3.2	72.5 ± 4.0	56.2 ± 2.7	62.5 ± 2.8	51.1 ± 2.5	55.5 ± 4.6	36.2 ± 0.5
$v \sin i_\star$ [km/s]	9.1 ± 1.0	2.7 ± 1.0	3.5 ± 1.0	2.7 ± 1.0	3.4 ± 1.0	8.2 ± 1.0	2.8 ± 1.0	2.9 ± 1.0
[Fe/H]	+0.15 ± 0.04	−0.12 ± 0.02	+0.04 ± 0.02	−0.26 ± 0.03	−0.17 ± 0.02	+0.05 ± 0.02	+0.25 ± 0.04	+0.35 ± 0.03
$\log R'_{\rm HK}$	−5.00 ± 0.13	−5.07 ± 0.21	−5.36 ± 0.33	−5.02 ± 0.19	−5.17 ± 0.24	−4.43 ± 0.10	−4.60 ± 0.10	−5.26 ± 0.24
$P_{\rm rot}$ [days]	11 ± 3	42 ± 11	28 ± 9	43 ± 11	22 ± 6	7 ± 4	19 ± 7	49 ± 12
$T_{\rm eff}$ [K]	6380 ± 60	5530 ± 35	6060 ± 30	5180 ± 45	5960 ± 20	5920 ± 30	5460 ± 50	5600 ± 40
$\log g$ [cgs]	4.37 ± 0.04	4.45 ± 0.03	4.24 ± 0.03	4.43 ± 0.10	4.24 ± 0.02	4.65 ± 0.05	4.47 ± 0.08	4.28 ± 0.05
Mass [$M_\odot$]	1.51 ± 0.11	0.87 ± 0.06	1.15 ± 0.08	0.78 ± 0.06	1.13 ± 0.06	1.01 ± 0.03	0.93 ± 0.07	1.07 ± 0.08

†: From Simbad.

The activity levels of the stars were evaluated from the Ca II emission index $\log R'_{\rm HK}$. The reported values and uncertainties are the averages and dispersions of values measured on each epoch for a given star. We note that the stars with the highest values of $\log R'_{\rm HK}$ are those for which that index shows the less dispersion with time. This could be surprising as active stars are expected to have larger variations of $\log R'_{\rm HK}$ than quiet stars. Here the larger uncertainties in $\log R'_{\rm HK}$ values of inactive stars is due to the larger dispersion they show due to the lower signal-to-noise ratios in the center of the cores of their H and K Ca II lines. Active stars have stronger flux in those lines, which implies larger signal-to-noise ratios and smaller dispersions. The three stars that present the lowest $\log R'_{\rm HK}$ also have lower $\log g$ values. This could be a sign that these stars are beginning their evolution to be sub-giants, for which the $\log R'_{\rm HK}$ calibration is not effective. As shown in Fig. 3, only two stars, namely HD 12484 and HIP 65407, show detectable chromospheric emissions. They are the two only ones among the eight stars to have $\log R'_{\rm HK}$ above −4.7 and considered here as active. According to Santos et al. (2000b), their levels of activity should induce stellar jitters of the order of 20 and 10 m/s, respectively. The low activity levels of the six remaining stars should imply stellar jitters of a few m/s at most.

According to Noyes et al. (1984) and Mamajek & Hillenbrand (2008), these levels of activity imply stellar rotation periods $P_{\rm rot}$ around 11, 7, and 20 days for HD 143105, HD 12484, and HIP 65407, respectively, and between 20 and 60 days for the five less active stars. The uncertainties related to these $P_{\rm rot}$ estimations are difficult to quantify. Those reported in Table 2 are estimations taking into account the uncertainties on our measured $\log R'_{\rm HK}$ and a ±0.16 uncertainty on the Rossby numbers (Mamajek & Hillenbrand 2008). These estimations of stellar rotation periods roughly agree with the upper limits derived from the $v \sin i_\star$ (Bouchy et al. 2005a) except for HIP 109600, HIP 109384, and HD 141399. They are different from the orbital periods measured below for the planets, so there are no hints that the periodic signals in radial velocities could be due to stellar activity modulated by star rotation. One possible exception is the inner planet of HIP 65407, which is discussed below in Sect. 5.1.2.

Stellar activity could also causes low-frequency radial-velocity variations due to magnetic cycles (see, e.g. Wright et al. 2008; Fares et al. 2009; Moutou et al. 2011; Carolo et al. 2014). For active stars, this can induce radial velocity variations up to 20 to 30 m/s. The shortest known magnetic cycles have periods of about two years and most of them are longer (22 years for the Sun). The periodicities we report below for our two active stars are shorter than 100 days, so they are unlikely to be due to magnetic cycles. Magnetic cycles have also been identified in inactive stars, with amplitudes up to a few m/s (Lovis et al. 2011). Four of our six inactive stars show periodicities shorter than 240 days, so they are unlikely to be caused by magnetic cycles. Our two remaining inactive stars (namely HIP 109384 and HD 141399) show radial velocity variations with longer periods. According Lovis et al. (2011), the amplitude of their magnetic cycles should be of the order of 1 m/s or below. Thus, magnetic cycles are unlikely to cause the larger variations we report.

4. Single-planet systems detection and characterization

4.1. Method

We describe here the orbit analyses of the six stars presenting only a single characterized planet: HD 143105, HIP 109600, HD 35759, HIP 109384, HD 220842, and HD 12484. For each of them the radial velocities present periodic variations which were already identified since the first ∼ 10 to ∼ 20 SOPHIE spectra were obtained. The following measurements allowed the periods to be confirmed for each object, and the parameters to be refined. We fitted the six final radial velocity sets with single Keplerian orbits using the procedure `yorbit` (Ségransan et al. 2011; Bouchy et al. 2016). The six parameters of the orbits are free to vary during the fits. In cases of objects with both SOPHIE and SOPHIE+ data, we introduced one extra free parameter in order to take into account for the possible radial velocity shift between both datasets. The radial velocity shifts we found (see below) agree with the values found by Moutou et al. (2014) and Wilson et al. (2016) between SOPHIE and SOPHIE+ (see however the particular case of HIP 109384 in Sect. 4.5). Finally, we allowed radial velocity linear drifts in addition to the Keplerian motions which added one extra free parameter for each object. Only one significant drift was detected (at more than 3σ), in the case of HD 220842. The free shift between SOPHIE and SOPHIE+ is unlikely to hide any possible actual stellar drift, except maybe in the case of HIP 109384 (Sect. 4.5).

Lomb-Scargle periodograms of the datasets show clear peaks at the periods of each orbit. Some additional peaks are also visible, corresponding to aliases or secondary lobes due to the sampling. The additional peaks all present smaller power than the main peaks, and Keplerian fits at these periods are clearly less good than the Keplerian fits made at the periods corresponding to the main peaks. So there are no ambiguities in the periods of the six detected planets. Periodograms of the radial velocities

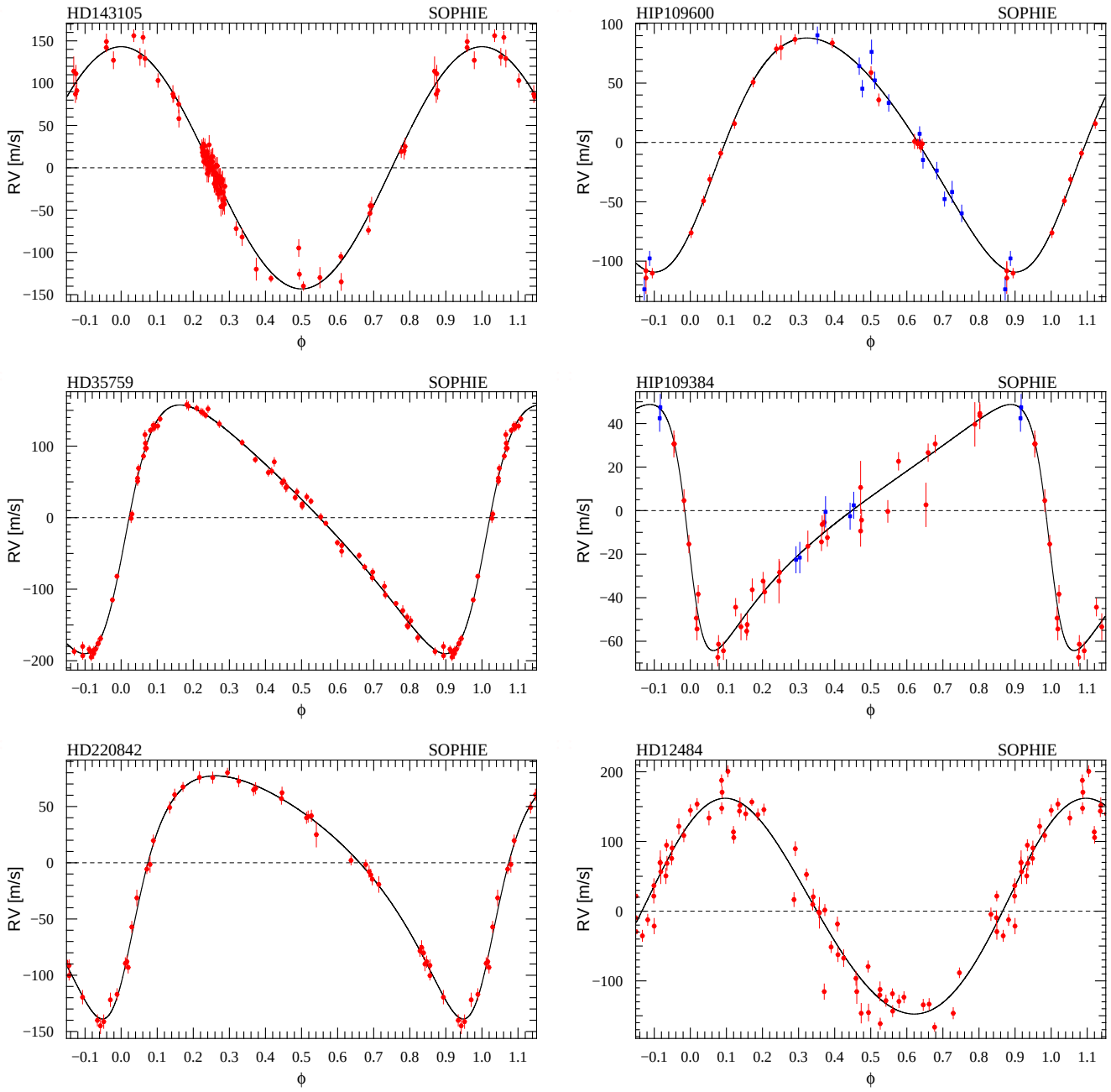

Fig. 4. Phase-folded radial velocity curves for the six stars with a single-planet detection. The SOPHIE data obtained before/after the June-2011 upgrade are plotted in blue/red with 1-σ error bars, and the Keplerian fits are the solid lines. The orbital parameters corresponding to the Keplerian fits are reported in Table 3. In the cases of HD 220842 the linear drift is subtracted here. The HD 143105b transit detection attempt of 2013-09-17 is shown around $\phi = 0.25$.

residuals after Keplerian fits show no significant peaks. The current data show no significant detections of extra companions in addition to the six single planets presented here, with the exception of the linear drift detected in HD 220842.

The derived orbital parameters of the six single planets are reported in Table 3 together with error bars which were computed from Monte Carlo and residuals permutation experiments both based on error bars on each radial velocity measurement. They provide similar error bars with no significant asymmetries or skews. We finally adopt the most conservative uncertainties. Table 3 includes the orbital period P, the eccentricity e, the argument of periastron ω, the time T_0 at periastron (or time of possible transits for circular or nearly circular orbits of HD 143105b and HD 12484b), the semi-amplitude K, le sky-projected mass of the planet $M_{\rm p} \sin i$, the semi-major axis a, the systemic radial velocities V_r, the number N of radial velocities and their time span, the dispersion $\sigma_{\rm O-C}$ of the residuals to the Keplerian fit, and the additional radial velocity drift (or its limit). The uncertainties on $M_{\rm p} \sin i$ and a are mainly due to the uncertainties on the host-star masses. The fits and their residuals are plotted as a function of time in the six upper panels of Fig. 2; the phase-folded plots are displayed in Fig. 4.

The Keplerian fits of the radial velocities provide measurements of the sky-projected mass $M_{\rm p} \sin i$ of the planetary com-

panions while the inclination i of the orbit remains unknown. Large masses for the companions could not formally be excluded from the radial velocities in cases of particularly small inclinations. In order to identify possible face-on systems we searched for signatures of orbital motion in Hipparcos astrometric data. Our stars have each between 100 and 150 Hipparcos measurements covering several periods of each planet, with a typical accuracy of a few mas. They were fitted with 5-parameter models using the orbital parameters obtained from the radial velocities, following the method described in details by Sahlmann et al. (2011). This method has proven to be reliable in detecting astrometric orbital signatures (e.g. Sahlmann et al. 2011, 2013; Díaz et al. 2012; Wilson et al. 2016). Here we detected no orbital motions. The corresponding upper limits $M_{\rm p\,max}$ on the companion masses are reported in the bottom line of Table 3. They are not really constraining. Any companion with a true mass around one Solar mass or above would have been detected as a secondary peak in the CCFs or as a variation in their bisectors, which is not the case here. We can however conclude here that none of our companions is an obvious binary in a face-on system.

The six single planetary systems are discussed below.

4.2. HD 143105

4.2.1. Keplerian fit

HD 143105 (BD +69°825, HIP 77838) is a rotating star ($v \sin i_\star = 9.1 \pm 1.0$ km/s) but does not show high activity level ($\log R'_{\rm HK} = -5.00 \pm 0.13$). Simbad classifies it as an F5 star but our temperature measurement ($T_{\rm eff} = 6380 \pm 60$ K; Sect. 3) suggests the slightly later spectral type F7. We started observing it in July 2013, after the SOPHIE+ upgrade. The star rapidly showed the typical signature of a hot Jupiter, with variation of $K \sim 150$ m/s and a period near 2.2 days. We followed that star for 14 months in order to confirm the detection, constrain the properties of the system, and detect any possible additional companion. The final dataset includes $N = 100$ radial velocity measurements that we fitted with Keplerian models. They did not provide a significant detection of any eccentricity: we measured $e = 0.021 \pm 0.016$ and $\omega = 40 \pm 70°$. The 3-σ upper limit we derived is $e < 0.07$. In agreement with the data and the fact that hot Jupiters are expected to be circularized, we assumed a circular orbit for the final fit. The derived radial velocity semi-amplitude is $K = 144.0 \pm 2.6$ m/s corresponding to a mass $M_{\rm p} \sin i = 1.21 \pm 0.06\,{\rm M_{Jup}}$. The planet HD 143105b orbits a slightly metal-rich star, in agreement with the tendency found for stars harboring Jupiter-mass planets (see, e.g., Santos et al. 2005).

The residuals around the Keplerian fit show a dispersion of 10.6 m/s. That quite large value is not due to the activity level of the star, which is low, nor the assumption for a circular orbit. That dispersion is mainly explained by the uncertainties of the radial velocities which is 9.2 m/s on average. The relatively low level of radial velocity accuracy obtained for that star by comparison to the other ones is due to the broadening of the lines cause by the stellar rotation. Moreover, HD 143105 is the hottest among the eight stars studied here and granulation effects might be higher. No significant linear drift nor particular structures were found in the residuals as a function of the time.

4.2.2. Transit search

Following 55 Cancri, HD 143105 is the second brightest star known to host a planet with a period shorter than three days (55 Cancri e being a super-Earth). Since HD 143105 is bright and the transit probability as high as 14 % for its hot Jupiter, that system was particularly interesting for photometric follow-up studies. So after the first SOPHIE observations on that star in July 2013 which rapidly showed it hosts a hot Jupiter, we started a transit search the following month using three different telescopes: Oversky, CROW, and ROTAT.

The Oversky Observatory (35 cm f/11 Schmidt-Cassegrain) telescope unfortunately had bad weather and the photometry could not be used to constrain any transit model. The CROW observatory in Portugal (28 cm f/10 Schmidt-Cassegrain, KAF1603ME CCD, 25 sec exposures, *Ic* filter, defocused images) produced three photometric series on August 15, August 26, and September 17, 2013. The dispersions are 4.0, 3.7, and 4.6 mmag, respectively, and 2.3, 2.1, and 2.7 mmag when data are binned to have a point approximatively every 120 sec. The ROTAT telescope at OHP (60 cm f/3.2 Newton, KAI11000M CCD) was also used for three nights in 2013: August 26 (4-sec exposures, Luminance filter, defocused images), September 6 (20-sec exposures, *R* filter, defocused images), and September 17 (4.5-sec exposures, Luminance filter, defocused images). On September 6, the dispersion is 10.7 mmag, and 7.8 mmag when binned to have a point approximatively every 120 sec. On September 17, cirrus were present sometimes and the dispersion is 20.1 mmag, and 8.1 mmag when binned.

The light curves are shown in Fig. 5 (upper panel). Differential photometry has been measured and the data have been detrended with smooth second order polynomials. Assuming a stellar radius $1.15\,{\rm R_\odot}$ typic of a F5V star, values for a and P from Table 3, and a central transit (impact parameter $b = 0$), we evaluate the transit maximum duration to ~ 2.37 hours, i.e. between transit phases -0.022 and $+0.022$. The uncertainty on the epoch of each transit mid-time is of the order of ±10 minutes (see Table 3). A light drop of about 15 mmag has been observed with ROTAT for about one hour on August 26 at the expected time of transit (these data were not detrended as they show that feature). Outside that event, the dispersion is 7.3 mmag, or 3.1 mmag when binned. Comparison stars (significantly fainter) do not show such event, so the hint for a transit detection was high. However, that event has not been observed at the other dates. Even more, the CROW observation secured on August 26 did not show the feature seen with ROTAT the same night. We conclude thus that no transit deeper than 10 mmag was detected. The event observed with ROTAT remains unexplained. A possibility could be a sporadic event due to stellar activity accidentally occurring at the time of of possible transit.

On September 17 the reality of the transit was still unclear, so we attempted a spectroscopic detection of the transit with SOPHIE through the Rossiter-McLaughlin effect (e.g. Hébrard et al. 2011). As the star is rotating ($v \sin i_\star = 9.1 \pm 1.0$ km/s), the amplitude of the Rossiter-McLaughlin anomaly is expected to be as high as ~ 100 m/s and thus easily detectable. No deviation from the Keplerian curve was detected during that night however (see upper-left panel of Fig. 4 and lower panel of Fig. 5). So, even if a transiting planet on a polar orbit and a null impact parameter would produce no Rossiter-McLaughlin signal, this scenario remains unlikely and we keep the conclusion that the planet is not transiting. The radial velocities obtained during the

September-17 night are used in the Keplerian fit presented above in Sect. 4.2.1.

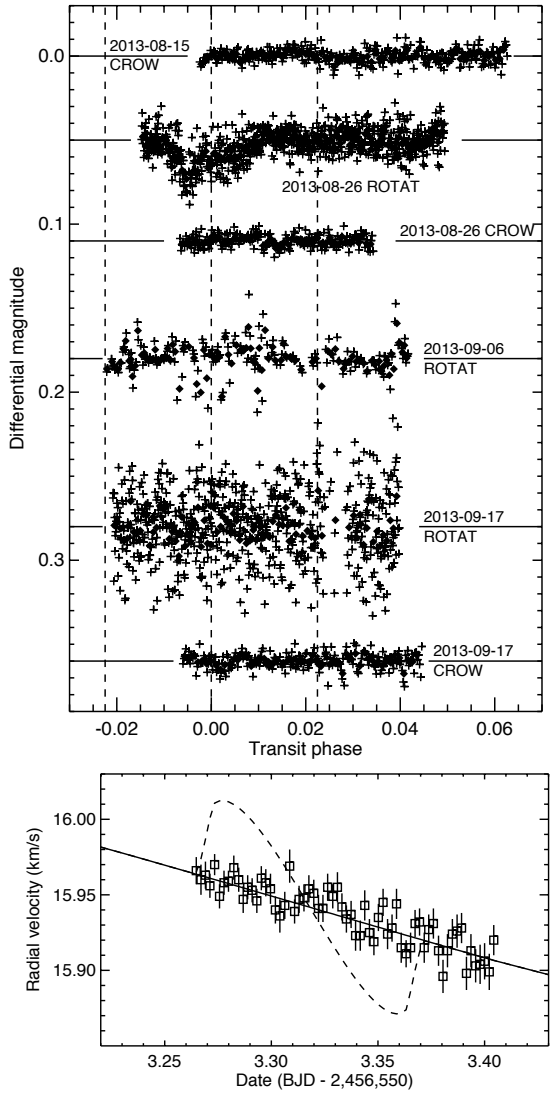

Fig. 5. Search for transits of HD 143105b. *Top: photometry*. The differential photometry is plotted as a function of the phase of the searched transits. The telescopes (CROW or ROTAT) and the dates are indicated for each of the six observations, which have been shifted in *y*-axes for clarity. The horizontal lines represents the mean of the data (or mean outside the event for 2013-08-26 with ROTAT). The original data (plus signs) have been binned to have a point approximatively every 120 seconds (diamond signs) to help their comparison. The vertical dashed lines represent the hypothetical ingress, center, and egress phases for central transits. The transit-like event observed on 2013-08-26 with ROTAT was not confirmed by other observations. *Bottom: spectroscopy*. SOPHIE radial velocities measured during a possible transit (2013-09-17). The expected Rossiter-McLaughlin anomaly is shown in dotted line (in case of aligned, prograde orbit); it is not detected. The solid line shows the Keplerian model with no transit (Figs. 2 and 4, Table 3).

4.2.3. Hot Jupiters around bright stars

With a magnitude $m_v = 6.75$, HD 143105 is one of the brightest stars known to host a hot Jupiter. Figure 6 shows the V magnitudes of hot-Jupiter host stars as a function of the year of their discovery, distinguishing transiting planets from those only characterized from radial velocities. Here hot Jupiters are defined as planets with $M_{\rm p} \sin i > 0.2\,{\rm M_{Jup}}$ and orbital periods shorter than 6 days, as suggested by mass and period distributions of known planets. In the continuation of the three first discovered hot Jupiters, 51 Peg b, Tau Boo b, and Ups And b (Mayor & Queloz 1995; Butler et al. 1997), the first decade of radial velocity surveys allowed about a dozen hot Jupiters to be discovered around stars brighter than $V = 8$. Three of them afterward turned out to transit, namely HD 209458b, HD 189733b, and HD 149026b (Charbonneau et al. 2000; Bouchy et al. 2005b; Sato et al. 2005). The transits in front of these three bright stars allowed numerous and important follow-up studies. The second decade allowed a plenty of hot Jupiters to be detected directly in transit from ground- and space-based photometric surveys in front of fainter stars. Still, Fig. 6 shows that radial velocity surveys continue to detect hot Jupiters in front of bright stars, and thus they are not all known. The transit probability being around 10 % for a hot Jupiter, it might remain transiting hot Jupiters to discover in front of bright stars, which would be of high interest for follow-up studies. They could be detected from radial velocity surveys, or later from the future TESS and PLATO satellites. It is possible that HD 143105b has been missed by some previous radial velocity surveys in case they avoided observing fast rotators. As shown here however, a stellar rotation of the order of $v \sin i_\star \sim 9$ km/s does not prevent at all hot Jupiters detection from radial velocities.

Orbiting a bright star, HD 143105b will be a precious object for follow-up in various spectral domains despite its non-transiting nature. If the planet has a grazing incidence, it may be possible to detect in the ultraviolet the partial transit of an evaporating atmosphere, extended by the high irradiation from

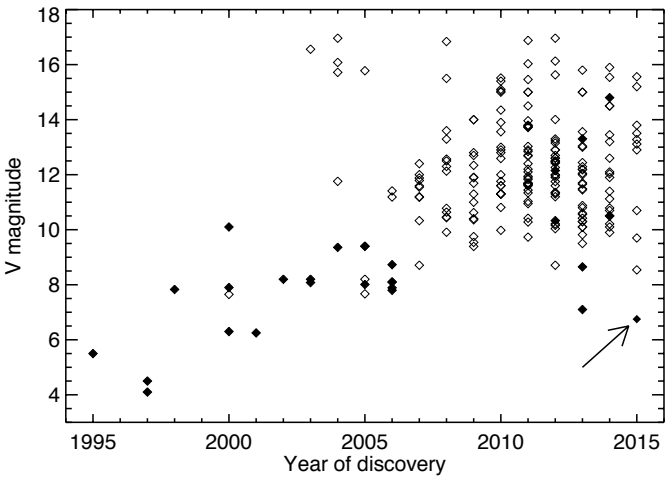

Fig. 6. Magnitudes of known hot-Jupiters host stars as a function of the planet discovery year. Transiting systems are empty symbols whereas non-transiting systems detected only in radial velocities are filled. Hot Jupiters are selected from exoplanets.org as planets with masses $> 0.2\,{\rm M_{Jup}}$ and periods < 6 days (220 planets). The host star of the new hot Jupiter HD 143105b is indicated with an arrow.

Table 3. Fitted Keplerian orbits and planetary parameters for the six single-planet system, with 1-σ error bars.

Parameters	HD 143105b	HIP 109600b	HD 35759b	HIP 109384b	HD 220842b	HD 12484b
P [days]	2.1974 ± 0.0003	232.08 ± 0.15	82.467 ± 0.019	499.48 ± 0.32	218.47 ± 0.19	58.83 ± 0.08
e	< 0.07	0.163 ± 0.006	0.389 ± 0.006	0.549 ± 0.003	0.404 ± 0.009	0.07 ± 0.03
ω [°]	–	−131.3 ± 1.6	−104.0 ± 1.3	104.49 ± 0.37	−134.9 ± 1.7	−35 ± 40
T_0 [BJD]‡	56531.344 ± 0.007	56017.1 ± 1.1	56469.72 ± 0.24	56337.02 ± 0.34	56624.8 ± 0.8	56699 ± 5
K [m s^{-1}]	144.0 ± 2.6	98.6 ± 0.5	173.9 ± 1.3	56.53 ± 0.22	108.1 ± 1.2	155 ± 5
$M_\mathrm{p} \sin i$ [M_Jup]†	1.21 ± 0.06	2.68 ± 0.12	3.76 ± 0.17	1.56 ± 0.08	3.18 ± 0.15	2.98 ± 0.14
a [AU]†	0.0379 ± 0.0009	0.706 ± 0.016	0.389 ± 0.009	1.134 ± 0.029	0.740 ± 0.018	0.297 ± 0.005
$V_{r,\mathrm{SOPHIE}}$ [km/s]	–	−70.0300 ± 0.0009	–	−63.6852 ± 0.0004	–	–
$V_{r,\mathrm{SOPHIE+}}$ [km/s]	15.9418 ± 0.0030	−69.9964 ± 0.0006	−12.5704 ± 0.0015	−63.6784 ± 0.0003	−22.5746 ± 0.0016	4.960 ± 0.005
N	100	34	71	42	42	65
$\sigma_{\mathrm{O-C,SOPHIE}}$ [m s^{-1}]	–	9.6	–	3.7	–	–
$\sigma_{\mathrm{O-C,SOPHIE+}}$ [m s^{-1}]	10.6	3.3	6.0	5.8	4.5	25.2
RV drift [m s^{-1} yr^{-1}]*	[−1.1; +12.5]	[−0.2; +12.0]	[−0.4; +4.5]	[−2.2; +1.5]	−35.5 ± 1.0 **	[−4.8; +32.3]
span [days]	422	2496	1261	2776	997	865
$M_{\mathrm{p\,max}}$[$M_\odot$]	14.65	0.43	1.04	0.27	0.35	0.96

‡: time at periastron for eccentric orbits; time of possible transits in the cases of the circular or nearly circular orbits of HD 143105b and HD 12484b.
†: using the stellar mass and its uncertainty from Table 2.
∗: significant RV drift detected only for HD 220842; 3-σ confidence intervals for other systems.
∗∗: the RV drift of HD 220842 is due to a substellar companion (see Sect. 4.6).

the F-type host star (see the case of 55 Cnc b; Ehrenreich et al. 2012). The inclination of the HD 143105b orbit could be constrained by measuring the polarization of its optical phase curve (Madhusudhan & Burrows 2012). Such measurements are challenging in the optical (e.g. Charbonneau et al. 1999; Leigh et al. 2003) where hot Jupiters have usually low albedos and yield faint signals. A tentative detection of phase variations from the non-transiting Saturn-mass planet HD 46375b was nonetheless obtained from CoRoT observations in the optical (Gaulme et al. 2010). Because the mass of HD 143105b is larger and orbits a brighter star at a similar orbital distance, its reflected light will probably be measurable at visible wavelengths with ultra-high precision photometry, e.g. with the future CHEOPS satellite. Despite the degeneracy caused by the absence of transit (the amplitude of the modulation varies as the product of the planet surface and geometric albedo), the shape and offset of the phase curve could reveal the composition and structure of the atmosphere (see, e.g., Seager et al. 2000; Showman & Guillot 2002; Heng & Demory 2013). It might already be possible to analyse the light reflected by HD 143105b atmosphere through cross-correlation of high-resolution optical spectra, constraining the planet orbital inclination and its true mass (Martins et al. 2013, 2015). High-resolution spectra of HD 143105b thermal emission from the dayside could be obtained in the future with infrared instruments as SPIRou at CFHT or JWST. The identification of individual molecular lines in the infrared would then bring further constraints on the thermal structure, the circulation, and composition of the atmosphere (e.g. Brogi et al. 2012; Snellen et al. 2014).

4.3. HIP 109600

The star HIP 109600 (BD +28°4312) was observed before and after the SOPHIE upgrade. We finally secured 34 measurements. The 232-day period is obvious on the time series, and no significant drift is detected over the nearly seven years of observation. The residuals of the Keplerian fit shows dispersions of 9.6 and 3.3 m/s for SOPHIE and SOPHIE+, respectively, in agreement with the typical uncertainties of their measurements. SOPHIE data are redshifted by 33.6±1.1 m/s by comparison to SOPHIE+.

The semi-amplitude is $K = 98.6 \pm 0.5$ m/s which corresponds to $M_\mathrm{p} \sin i = 2.68 \pm 0.12\,M_\mathrm{Jup}$. HIP 109600b is a giant planet orbiting a G5V star in $P = 232.08 \pm 0.15$ days with a low but significant eccentricity of $e = 0.163 \pm 0.006$. Its orbit is thus located in a temperate orbit, with an insolation level around 1.5± 0.3 that of the Earth on its orbit. The habitable zone around a star could be defined as the area where the insolation level would be between 0.2 and 1.8 that of the Earth (e.g. Kopparapu et al. 2013; Jenkins et al. 2015). Any possible satellite orbiting HIP 109600b could thus be habitable. The presence of such satellites remains out of reach of present technics unfortunately. We note also that HIP 109600 is metal-poor ([Fe/H] = −0.12 ± 0.02), whereas most giant-planet hosts are metal-rich.

Several studies have shown that the Keplerian signature of a single, eccentric planet could also be fitted with a model including two planets on circular (or nearly circular) orbits in 2:1 resonance, depending on the radial velocity accuracy and their time sampling (e.g. Anglada-Escudé et al. 2010; Wittenmyer et al. 2013; Kürster et al. 2015). Numerous pairs of planets near the 2:1 orbital resonance have indeed be detected in transit with *Kepler* (e.g. Lissauer et al. 2011; Delisle & Laskar 2014). Here, adding an inner planet with a period half of the HIP 109600b one provides a fit with a similar residuals dispersion than the one-planet fit adopted above. So residuals dispersion comparison does not allow us to exclude the presence of an inner planet with a period of ∼ 117 days and a semi-amplitude $K = 16 \pm 2$ m/s corresponding to $M_\mathrm{p} \sin i = 0.35 \pm 0.04\,M_\mathrm{Jup}$. Adding that additional, inner planet would not significantly change the parameters of HIP 109600b, except its orbit is circular.

To compare further the above one- and two-planet Keplerian models, we computed their Bayesian evidences using the methods of Chib & Jeliazkov (2001) and Perrakis et al. (2014) (see also Díaz et al. 2016b). Both methods produce similar results but the dispersion of Chib & Jeliazkov (2001) is much smaller. We found that the one-planet model is 21.9 ± 0.8 times more probable, so we finally adopt that solution.

4.4. HD 35759

We started observing HD 35759 (BD +64°532, HIP 25883) in September 2011, a few weeks after the SOPHIE+ upgrade. 71

radial velocities were finally acquired. Their Lomb-Scargle periodogram shows a clear peak at 82.5 days, as well as a weaker peak at the harmonic corresponding to half the period. There are no ambiguities however on the true period of the signal, measured to be 82.467 ± 0.019 days.

The Keplerian fit of the radial velocities provides a semi-amplitude $K = 173.9 \pm 1.3$ m/s corresponding to a mass $M_{\rm p} \sin i = 3.76 \pm 0.17\,{\rm M_{Jup}}$. The eccentricity is significantly detected to be $e = 0.389 \pm 0.006$. HD 35759b is thus a giant planet orbiting a G5V star with a period similar to that of Mercury but with a larger eccentricity.

The residuals of that fit show a dispersion of 6.0 m/s, in agreement with the typical accuracy of the measurements. Adding an inner planet in a circular orbit of half that period significantly degrades the fit, providing a residuals dispersion above 20 m/s. Moreover, we detect no significant drift over the 3.5 years of observation neither. So there are no hints for any additional inner nor outer companion in that system.

4.5. HIP 109384

We observed the G5V star HIP 109384 (BD +70°1218) over more than seven years, before and after the SOPHIE upgrade. The final dataset includes 42 measurements. The periodic signal with a period near 500 days clearly appears in the data. The residuals of the one-planet Keplerian fit are 3.7 and 5.8 m/s, in agreement with the uncertainties on the individual measurements with SOPHIE and SOPHIE+, respectively. The dispersion is surprisingly larger for data secured after the upgrade, but only seven measurements were secured before the upgrade. The SOPHIE data are redshifted by 6.7 ± 0.5 m/s by comparison to SOPHIE+, which is a small shift when compared to other systems observed before and after the upgrade, in the present study as well as in Moutou et al. (2014) or Wilson et al. (2016). This could be the signature of an additional drift due to another companion in the system, but the current data do not allow that to be confirmed. The Keplerian fits made with or without that drift provide similar parameters for the planet HIP 109384b. Adding a circular, inner planet with a period near 250 days (half the period of HIP 109384b) provides a significantly poorer fit with a residuals dispersion of 12 m/s for the SOPHIE+ data, so there are no hints for such an inner, additional planet in 2:1 resonance.

HIP 109384b has a mass $M_{\rm p} \sin i = 1.56 \pm 0.08\,{\rm M_{Jup}}$ ($K = 56.53 \pm 0.22$ m/s) and a period of 499.48 ± 0.32 days. Its host star is metal-poor ([Fe/H] = −0.26 ± 0.03). The orbit is eccentric with $e = 0.549 \pm 0.003$. In addition to the main signal of HIP 109384b, the Lomb-Scargle periodogram shows a weak peak near 10 days which is still visible in the residuals of the 1-planet fit. No corresponding peaks are seen in the periodograms of bisectors, width, nor $\log R'_{\rm HK}$. The residuals could be fitted at this period with an amplitude $K \simeq 6$ m/s, corresponding to about one Neptune mass; that small signal is not significant in our data however so we do not claim such a detection. We will continue observing that star in order to study that signal, as well as the possible drift. The presence or not of such additional inner or outer planet does not significantly change the parameters of the giant planet HIP 109384b.

From periastron and apoastron of its eccentric orbit, the insolation levels of HIP 109384b could be estimated between 0.4 ± 0.1 and 0.6 ± 0.1 of the Earth's insolation. This places HIP 109384b in the outer part of its habitable zone, making particularly interesting any satellite which might orbit that giant planet.

4.6. HD 220842

We started observing the F8V, inactive, metal-poor star HD 220842 (BD +56°3009, HIP 115714) in June 2012, one year after the SOPHIE upgrade. The dataset includes 42 radial velocity measurements spread over 2.7 years. They display large variations that can be fitted with a Keplerian orbit of 218-day period. Figure 2 could suggest that this period mainly stands on one point (at BJD = 2 456 847.6), and that a single planet on a period two times longer (about 440 days) could fit the data as well if that point is omitted. However, fits without that point and with a double period show clearly a larger dispersion in their residuals, and we found no reasons to omit that point.

The final fit provides a period of 218.47 ± 0.19 days and a semi-amplitude $K = 108.1 \pm 1.2$ m/s corresponding to the mass $M_{\rm p} \sin i = 3.18 \pm 0.15\,{\rm M_{Jup}}$. The residuals show a dispersion of 4.5 m/s in agreement with the accuracy of the measurements. The orbit is eccentric with $e = 0.404 \pm 0.009$. Including an additional, circular planet with a period near 109 days (half the period of HD 220842b) provides a significantly poorer fit with a residuals dispersion of 13 m/s, so there are no hints for such inner, resonant planet.

In addition to the one-planet Keplerian model, the data clearly show an additional drift revealing the presence of a second companion to the star, which could be stellar or planetary. There are no indications of binarity of that star in the literature. A linear trend is enough to fit the drift and we obtain $-35.5 \pm 1.0\,{\rm m\,s^{-1}\,yr^{-1}}$. Assuming an eccentricity of $e \simeq 0.5$ for that additional companion, it would correspond to a period of at least $\sim$ 1100 days and a projected mass of at least $\sim 2.1\,{\rm M_{Jup}}$. Solutions with longer periods and larger masses are also allowed from the data, as well as different values for the eccentricity. We will continue to follow that system with SOPHIE to characterize that second component, and in particular to determine if it is a planet or a star.

To search for the companion at the origin of the drift we observed HD 220842 with the Subaru Telescope Extreme Adaptive Optics system (SCExAO; Jovanovic et al. 2015). SCExAO is a high performance coronagraph using a series of wavefront controls at the 8-m Subaru Telescope in Mauna Kea (Hawaii, USA). HD 220842 was observed for 20 minutes on November 1st, 2015 in field rotation mode, and the angular differential imaging data was reduced using GRAPHIC (Hagelberg et al. 2016). No companion was detected in the resulting data but an upper limit on the putative companion can be derived from the detection limit (Fig. 7). The detection limit is generated following a similar procedure as in Chauvin et al. (2015), while the mass estimates are based on the BT-SETTL models (Allard et al. 2014) using a conservative age estimate of 5 Gyr for the system. Assuming the companion was not hidden below or in front of the star at the time of our observation, we can exclude at $5\,\sigma$ that the companion is more massive than $20\,{\rm M_{Jup}}$ with a period shorter than $\sim$ 230 years ($a \sim 60$ AU), or more massive than $40\,{\rm M_{Jup}}$ with a period shorter than $\sim$ 75 years ($a \sim 20$ AU). We can thus conclude that the companion at the origin of the linear drift is probably sub-stellar. Future observations could reinforce that conclusion if the companion remains undetected at different epochs. Deeper observations than the snapshot we have obtained may be able to directly detect the companion.

4.7. HD 12484

The F8V star HD 12484 (BD +02°320, HIP 9519) was observed with SOPHIE+ from September 2012 to January 2015. The

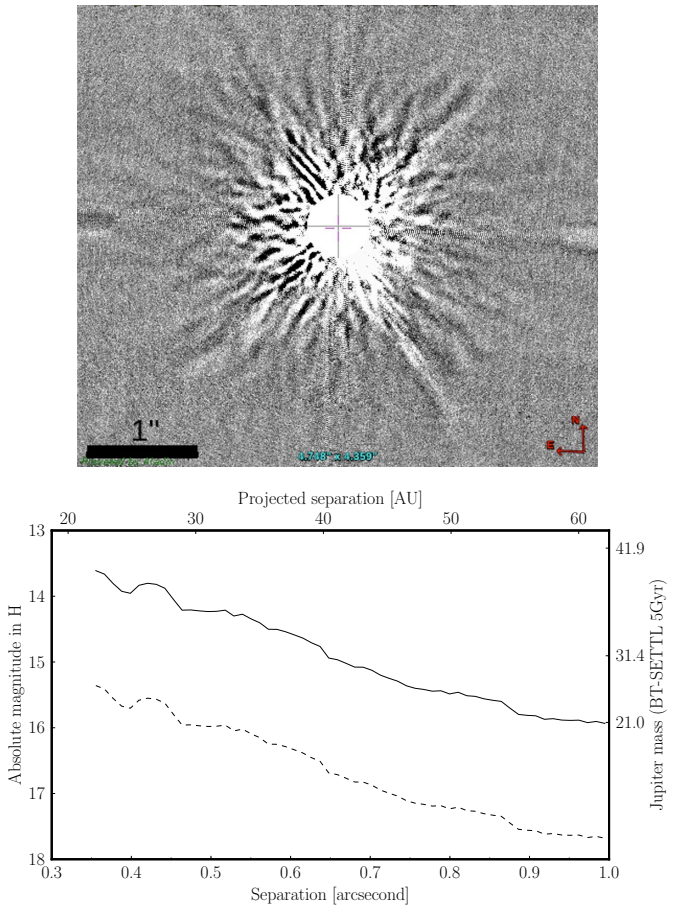

Fig. 7. Subaru/SCExAO ADI observation of HD 220842 in H-band (upper panel). No candidate has been resolved in this snapshot. The lower panel shows the corresponding upper limits on the companion producing the radial-velocity drift of HD 220842. Detections limits at 1 and 5 σ are plotted in dashed and solid lines, respectively. The mass estimate is based on BT-SETTL CIFIST2011 models (Allard et al. 2014). The contrast curve has been corrected to take into account self-subtraction. Companions above the solid line woulde have been detected at more than 5 σ.

final dataset includes 65 radial velocities with a typical accuracy of 10 m/s. The moderate level of accuracy is due to the broadening of the lines caused by the rotation of the star ($v \sin i_\star = 8.2 \pm 1.0$ km/s). That F8V star is active with chromospheric emissions in the H and K lines (Fig. 3) corresponding to $\log R'_{\rm HK} = -4.43 \pm 0.10$. Despite that high level of activity which implies stellar jitter, a periodic signal is clearly detected in the data. The one-planet Keplerian fit provides a period of 58.83 ± 0.08 days and a semi-amplitude $K = 155 \pm 5$ m/s corresponding to $M_{\rm p} \sin i = 2.98 \pm 0.14\,{\rm M_{Jup}}$. No significant eccentricity is detected and we obtained the formal value $e = 0.07 \pm 0.03$. The period being outside the domain range of hot Jupiters, there are no reasons to fix the orbit as circular, and we let the eccentricity free in the fit.

The dispersion of the residuals of the fit is 25.2 m/s which is large in comparison to the accuracy of the data. They agree however with the stellar jitter of ∼20 m/s expected for an F-type star at that level of activity (Santos et al. 2000b). Figure 8 shows the clear anti-correlation between the bisector spans and the radial velocity residuals after the Keplerian fit, which is the typical signature of variations induced by stellar activity (Queloz et al. 2001; Boisse et al. 2009). We thus conclude that the extra noise in the radial velocities is due to the stellar activity of HD 12484. No periodic signals were detected in the residuals, even by considering only short time spans of data. The rotation period deduced from the activity level of the star is $P_{\rm rot} \simeq 7 \pm 4$ days. It is different enough from the orbital period of the planet to assume that the activity noise does not significantly perturb the parameters of the planet. Indeed, the parameters are deduced from the Keplerian model which considers the stellar jitter as an uncorrelated noise, which is not necessary the case here.

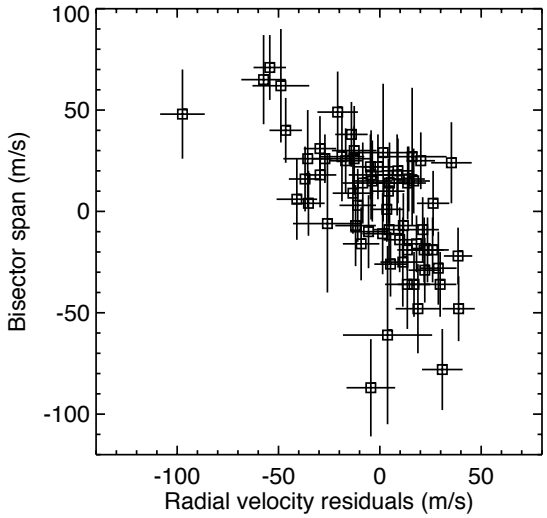

Fig. 8. Bisector span as a function of the the radial velocity residuals after the Keplerian fit for HD 12484. The clear anti-correlation indicates that the residuals are mainly due to the stellar activity.

The inclination of the orbit being unknown, the transit probability of HD 12484b is ∼ 1.5 %. Among the new single planets presented here, this is the second highest transit probability after the hot Jupiter HD 143105b (Sect. 4.2). The four other single planets presented above have transit probabilities included between 0.5 and 1.0 %. HD 143105b is the only one for which we have attempted a transit detection up to now.

Adding an inner planet with half the orbital period of HD 12484b provides a fit with a similarly high residuals dispersion of 25 m/s. This dispersion comparison does not exclude the presence around HD 12484 of an inner planet with a period of ∼ 29 days and semi-amplitude $K = 15 \pm 5$ m/s corresponding to $M_{\rm p} \sin i = 0.22 \pm 0.08\,{\rm M_{Jup}}$. However, Bayesian evidences comparison for both models (see Sect. 4.3) indicates that the one-planet model is 7.8 ± 0.5 times more probable than the two-planet model. So there is no evidence for the presence of such speculative inner, resonant planet, and we adopt the one-planet model for HD 12484.

Active stars known to host planets are sparse. This is likely to be a selection bias. Indeed, the stellar jitter caused by activity makes them unfavorable objects to detect planets so they are frequently excluded from radial velocity surveys searching extrasolar planets. Only a few planetary systems are known around stars with $\log R'_{\rm HK} > -4.5$. They include hot Jupiters as WASP-52b, 59b, or 84b (Hébrard et al. 2013; Anderson et al. 2014), giant planets on longer periods as HD 192263b, GJ 3021b, and

HD 81040b (Santos et al. 2000a; Naef et al. 2001; Sozzetti et al. 2006), or the multi-planet systems around HD 128311 and HD 9446 (Vogt et al 2005; Hébrard et al. 2010). The new giant planet HD 12484b increases that population.

5. Multi-planet systems detection and characterization

The two last systems presented in this paper show the signature of multi-planet systems: two planets around HIP 65407 and four around HD 141399. They add new cases among the few systems hosting several giant planets, whereas most of the low-mass planets are in multiple systems. Over the 535 systems from exoplanets.org known to include planet(s) with masses above 0.3 M_{Jup}, only 50 are multiple. After detection-bias corrections, Mayor et al. (2011) report multi-planetary rates of 26 % for giant planets and over 70 % for planets below 0.1 M_{Jup}.

We fitted the datasets of both multiple systems and determined the uncertainties on their parameters using the same Keplerian procedure as above for singe planets (Sect. 4.1), with five extra free parameters per additional planet. These Keplerian analyses do not take into account for any gravitational interactions between planets, which could be significant in some cases. So we subsequently complement the purely Keplerian analyses by additional dynamical studies and compare the results of both approaches. Our different analyses of both multi-planet systems are discussed below.

5.1. HIP 65407

5.1.1. Planets detection

We obtained 65 radial velocity measurements of HIP 65407 (BD +49°2212) over more than four years, both with SOPHIE and SOPHIE+. The data soon revealed the signature of two periodic variations in the planet-mass range, which were confirmed by subsequent SOPHIE observations.

Figure 9 shows Lomb-Scargle periodograms of the measurements and residuals of HIP 65407. In the upper panel of Fig. 9 that presents the periodogram of the radial velocities of HIP 65407, periodic signals at 28 days and 67 days are clearly detected with peaks at the periods corresponding to the two planets. The peaks around one day correspond to the aliases of both detected signals, as the sampling is as usual biased with the nights and days succession.

In the second panel of Fig. 9 is plotted the periodogram of the residuals after subtraction of a fit including only the 28-day-period planet. The peak at 67 days is visible in those residuals. In the same manner, the third panel of Fig. 9 shows the periodogram of the residuals after a fit including only the 67-day-period planet. The peak at 67 days is no longer visible and this time the peak at 28 days is visible. The bottom panel of Fig. 9 shows the periodogram of the residuals after subtraction of the Keplerian fit including both HIP 65407b and HIP 65407c. There are no remaining strong peaks on this periodogram; even the 1-day alias disappeared, showing that most of the periodic signals have been removed from the data. False-alarm probabilities of 1×10^{-3} are also reported in Fig. 9; they are based on bootstrap experiments, and comparisons of periodograms peaks among all periodograms obtained for each radial-velocity permutation.

This periodogram analysis shows that the two planets are clearly detected in our data with unambiguous periods, and that there are no significant additional periodic signals. In particular, there are no signs of additional planets at longer periods on the time span of our data (more than four years), which is also seen by the fact we do not detect any significant linear drift in the radial velocities in addition to the signature of the two planets.

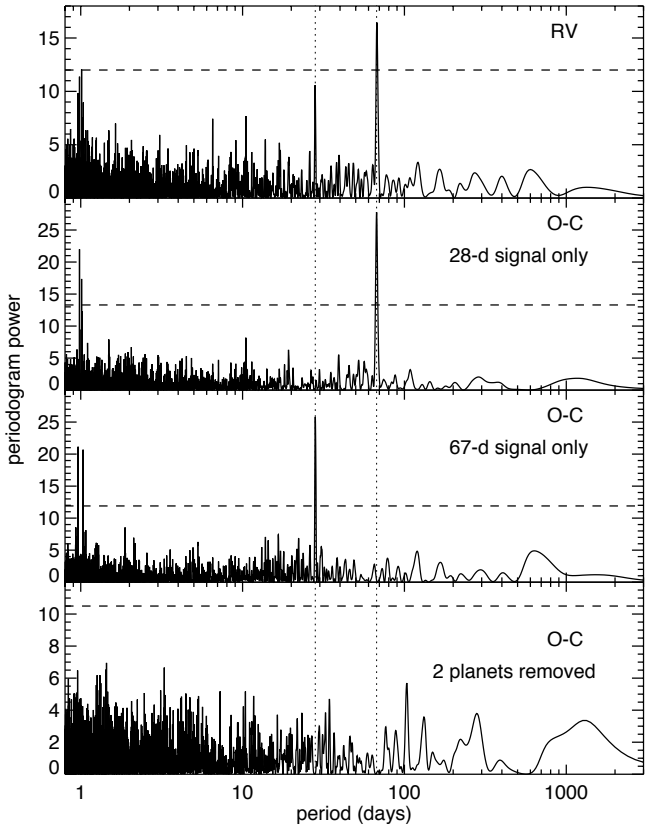

Fig. 9. Lomb-Scargle periodograms of the SOPHIE radial velocities of HIP 65407. The upper panel shows the periodogram computed on the radial velocities without any fit removed. The second and third panels show the periodograms computed on the residuals of the fits only including HIP 65407b or HIP 65407c, respectively. The bottom panel shows the periodogram after the subtraction of the two-planet fit. The two vertical dotted lines show the periods of the two planets. The horizontal dashed lines correspond to the false-alarm probability of 1×10^{-3}.

5.1.2. Keplerian fit

The radial velocities were first fitted with a Keplerian model, i.e. neglecting any possible gravitational interactions between both planets. The two-planet Keplerian best fit is plotted in Fig. 2 as a function of time (lower, left panel) and in Fig. 10 as function of the orbital phase. The different phases of both orbits are well covered by our observations. The derived parameters are reported in Table 4. The inner planet, HIP 65407b, produces radial velocity variations with a semi-amplitude $K = 30.5 \pm 1.6$ m/s corresponding to a planet with a minimum mass $M_p \sin i = 0.428 \pm 0.032$ M_{Jup}. Its orbit has a period of 28.125 ± 0.019 days and no significant detection of any eccentricity ($e = 0.14 \pm 0.07$). The outer planet, HIP 65407c, yields a semi-amplitude $K = 41.5 \pm 1.9$ m/s corresponding to a planet with a projected mass $M_p \sin i = 0.784 \pm 0.054$ M_{Jup}. The orbital period is 67.30 ± 0.08 days and there is a hint of a possible small eccentricity detection ($e = 0.12 \pm 0.04$). No astrometric motions cor-

Table 4. Fitted Keplerian orbits and planetary parameters for the two multi-planetary system, with 1-σ error bars.

Parameters	HIP 65407b	HIP 65407c	HD 141399b	HD 141399c	HD 141399d	HD 141399e
P [days]	28.125 ± 0.019	67.30 ± 0.08	94.44 ± 0.05	201.99 ± 0.08	1069.8 ± 6.7	5000^{+560}_{-2000} *
e	0.14 ± 0.07	0.12 ± 0.04	0.04 ± 0.02	0.048 ± 0.009	0.074 ± 0.025	0.26 ± 0.22*
ω [°]	50 ± 150	−19 ± 25	−90 ± 80	−140 ± 40	−140 ± 30	−10 ± 20
T_0 [BJD] ‡	56990.8 ± 2.5	57047 ± 6	56998 ± 15	56838 ± 10	56923 ± 65	58900 ± 800
K [m s^{-1}]	30.5 ± 1.6	41.5 ± 1.9	19.23 ± 0.47	44.20 ± 0.50	22.63 ± 0.59	8.8 ± 0.9
$M_p \sin i$ [M_{Jup}]†	0.428 ± 0.032	0.784 ± 0.054	0.451 ± 0.030	1.33 ± 0.08	1.18 ± 0.08	0.66 ± 0.10
a [AU]†	0.177 ± 0.005	0.316 ± 0.008	0.415 ± 0.011	0.689 ± 0.020	2.09 ± 0.06	5.0 ± 1.5
$V_{r,\mathrm{SOPHIE}}$ [km/s]	−8.748 ± 0.005			−21.566 ± 0.002		
$V_{r,\mathrm{SOPHIE+}}$ [km/s] [km/s]	−8.720 ± 0.003			−21.548 ± 0.001		
N	65			139		
$\sigma_{\mathrm{O-C,SOPHIE}}$ [m s^{-1}]	11.9			12.8		
$\sigma_{\mathrm{O-C,SOPHIE+}}$ [m s^{-1}]	7.5			4.8		
RV drift [m s^{-1} yr^{-1}]	[−0.6; +7.8]			[−1.3; +2.4]		
span [days]	1517			2566		
$M_{p\,max}$[$M_\odot$]	8.11	2.25	0.22	0.12	0.04	–

‡: time of possible transits.
†: using the stellar mass and its uncertainty from Table 2.
∗: stability analyses of HD 141399e provide P_e = 3370 ± 90 days and e_e < 0.1 (see Sect. 5.2.2).

responding to these planets were detected in the Hipparcos data (Sect. 4), in agreement with the non-detection of any secondary peak in the CCFs. The derived upper limits $M_{p\,max}$ on the planetary masses are above one Solar mass and thus not constraining.

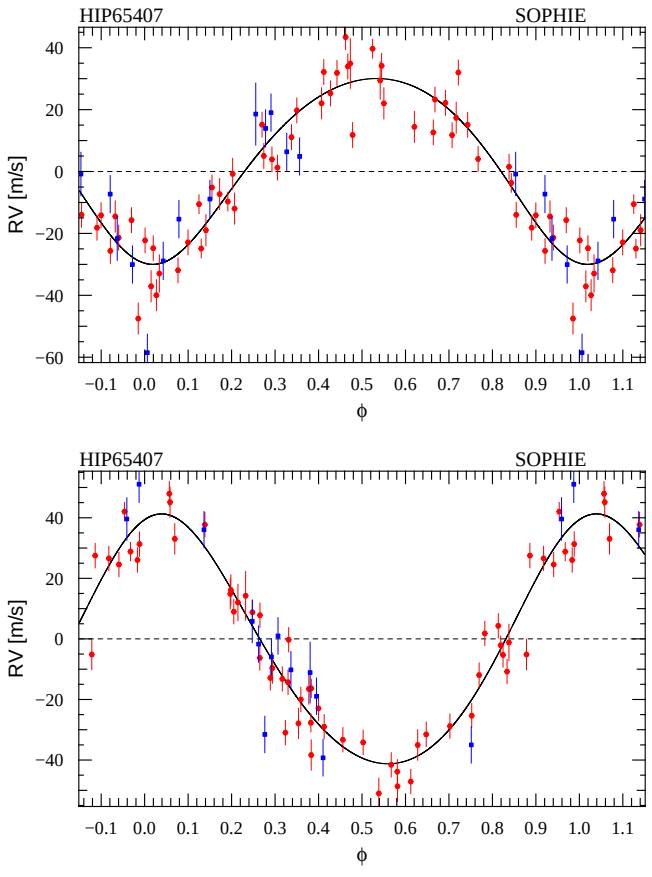

Fig. 10. Phase-folded radial velocity curves for HIP 65407b (P = 28.1 d, top) and HIP 65407c (P = 67.3 d, bottom) after removing the effect of the other planet. The SOPHIE data obtained before/after the June-2011 upgrade are plotted in blue/red with 1-σ error bars, and the Keplerian fits are the solid lines. Orbital parameters corresponding to the fits are reported in Table 4.

SOPHIE data are redshifted by 20.0 ± 5.8 m/s by comparison to SOPHIE+. There are mainly SOPHIE+ data for that system and their residuals show a better dispersion (7.5 m/s) than that of SOPHIE residuals (11.9 m/s). That dispersion is slightly larger than the one expected for SOPHIE+. This could be partly due to stellar jitter as the host star is active. Its $\log R'_{HK} = -4.60 \pm 0.10$ could imply stellar jitter of the order of 10 m/s (Sect. 3). In addition, the period of the inner planet (28.125 ± 0.019 days) is just slightly longer than the stellar rotation period, roughly estimated in Sect. 3 to be 19 ± 7 days. Confusions between stellar activity signals and Doppler wobble due to the planet could be suspected here. We note however that the bisectors show no significant variations, periodicity, or correlation as a function of the radial velocities, or as a function of the radial velocity residuals after fits including both planets or just one of them. Such correlation could have been the signature of changes in the stellar line profiles due to the activity of the star, as in the case of HD 12484 (Sect. 4.7). We do not see either any significant periodicities in the periodograms of Fig. 9 in addition to those of the two planets. This could have been the signature of stellar rotation. So despite the fact that the star is active, we detect no significant signs of stellar jitter in our radial velocity data, except possibly dispersion residuals that are slightly larger than expected. Moreover, the parameters of both planets are stable over the more than four years of observations; they also remain unchanged when only short-time sequences are analyzed instaed of the whole dataset. Together with the absence of periodicities in the periodograms of other activity indicators as the width of the CCF or the $\log R'_{HK}$ index, it is thus unlikely that the activity of the star does significantly affect the orbital parameters that we derived from their Keplerian fit. These parameters appear thus reliable.

The transit probabilities for HIP 65407b and HIP 65407c are ∼ 2.6 % and ∼ 1.3 %, respectively. We have not attempted any transit detection for them up to now.

As the system shows a planetary system composed of two planets in compact orbits, we assessed below the gravitational interactions between both planets in order to evaluate their possible effects and differences with the Keplerian fit which assumes both planets do not interact. The stability of the system is not straightforward since the minimum masses of the planets are

Table 5. Fundamental frequencies for the Keplerian orbital solution in Table 4. n_b and n_c are the mean motions, and g_1 and g_2 are the secular frequencies of the periastrons.

	Frequency (°/yr)	Period (yr)	Angle (ϕ_k) (deg)
n_b	4675	0.0770	21.89
n_c	1954	0.1843	-125.4
g_1	1.747	206.1	161.6
g_2	0.2568	1402	-32.66

of the same order as the mass of Jupiter. As a consequence, mutual gravitational interactions between planets may give rise to some instabilities.

5.1.3. Secular coupling

The ratio between the orbital periods determined by the Keplerian fit (Table 4) is $P_c/P_b = 2.4$, which is close to a 12:5 mean motion resonance. We performed a frequency analysis of the Keplerian orbital solution listed in Table 4 computed over 10 kyr. The orbits of the planets are integrated with the symplectic integrator SABAC4 of Laskar & Robutel (2001), using a step size of 0.01 yr. We concluded that, in spite of the proximity of the 12:5 mean motion resonance, the two planets in the HIP 65407 system are not trapped inside, at least when we adopt the minimum values for the masses.

The fundamental frequencies of the systems are then the mean motions n_b and n_c, and the two secular frequencies of the periastrons g_1 and g_2 (Table 5). Because of the proximity of the two orbits, there is a strong coupling within the secular system (see Laskar 1990). Both planets HIP 65407b and HIP 65407c precess with the same precession frequency g_1, which has a period of 206 years. The two periastrons are thus locked and $\Delta\omega = \omega_c - \omega_b$ oscillates around 180° (anti-aligned ellipses) with a maximal amplitude of about 45° (see Fig. 11).

To present the solution in a clearer way, it is useful to make a linear change of variables into eccentricity proper modes (Laskar 1990). In the present case, due to the proximity of the 12:5 mean motion resonance and due to the possible eccentric orbits, the linear transformation is numerically obtained by a frequency analysis of the solutions. Using the classical complex notation $z_p = e_p e^{i\omega_p}$, for $p = b, c$, we have for the linear Laplace-Lagrange solution:

$$\begin{pmatrix} z_b \\ z_c \end{pmatrix} = \begin{pmatrix} 0.1669 & 0.03924 \\ -0.06496 & 0.03307 \end{pmatrix} \begin{pmatrix} u_1 \\ u_2 \end{pmatrix} . \quad (1)$$

The proper modes u_k (with $k = 1, 2$) are obtained from the z_p by inverting the above linear relation. To good approximation, we have $u_k \approx e^{i(g_k t + \phi_k)}$, where g_k and ϕ_k are given in Table 5. From Eqs. 1, the meaning of the observed libration between the periastrons ω_b and ω_c could be understood. Indeed, for both planets HIP 65407b and HIP 65407c, the dominant term is u_1 with frequency g_1, and they thus both precess with an average value of g_1 (green line in Fig. 11).

Equations 1 usually also provide a good approximation for the long-term evolution of the eccentricities. In Fig. 12 we plot the eccentricity evolution with initial conditions from Table 4. Simultaneously, we plot with green lines the evolution of the same elements given by the above secular, linear approximation. We see nevertheless that there is a small deviation from the linear approximation. Going back to the decomposition of z_p in the proper modes, we notice that there is an additional forcing frequency at $2g_1 - g_2$ with significant power. We can correct the linear Laplace-Lagrange solution (Eqs. 1) to include the contribution from this term as:

$$\begin{pmatrix} z_b \\ z_c \end{pmatrix} = \begin{pmatrix} 0.1670 & 0.03924 & -0.005583 \\ -0.06496 & 0.03307 & 0.002529 \end{pmatrix} \begin{pmatrix} u_1 \\ u_2 \\ u_1^2 u_2^{-1} \end{pmatrix} . \quad (2)$$

In Figs. 11 and 12 we plot with black lines the evolution using the corrected secular approximation. We see there is now a

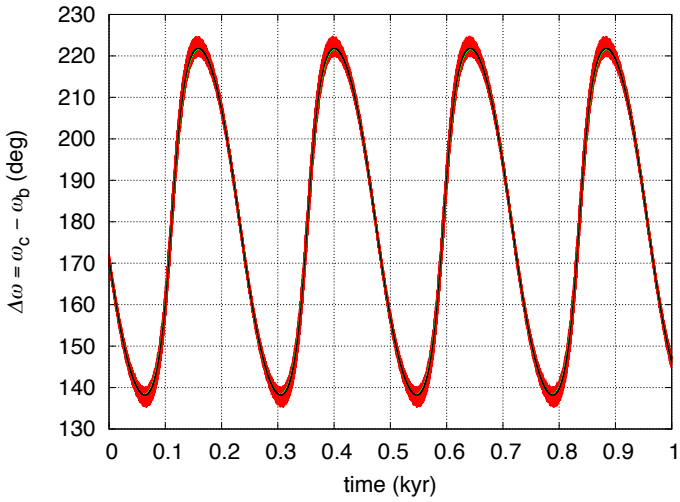

Fig. 11. Evolution in the HIP 65407 two-planet system of the angle $\Delta\omega = \omega_c - \omega_b$ (red line), which oscillates around 180° with a maximal amplitude of 45°. The green and black lines (nearly over-plotted) also gives the $\Delta\omega$ evolution, but obtained with the linear secular models (Eqs. 1 and 2, respectively).

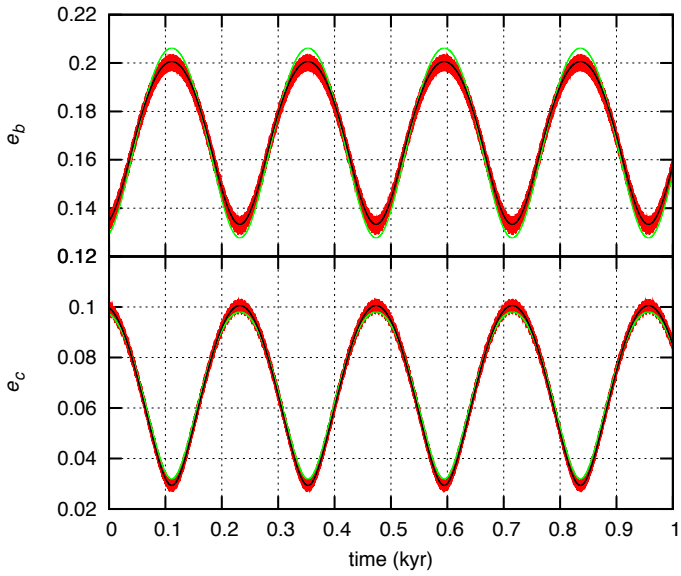

Fig. 12. Evolution with time of the eccentricities e_b and e_c of both planets HIP 65407b and HIP 65407c, starting with the orbital solution from Table 4. The red lines give the complete solutions for the eccentricities obtained numerically, while the green and black curves are the associated values obtained with the linear secular models (Eqs. 1 and 2, respectively).

perfect agreement with the numerical solution, so the term in $2g_1 - g_2$ is essential for the correct description of the secular evolution of the system. The eccentricity variations are limited and described well by the secular approximation (Eqs. 2). The eccentricity of planets HIP 65407b and HIP 65407c are within the ranges $0.129 < e_b < 0.204$ and $0.027 < e_c < 0.103$, respectively. These variations are driven mostly by the secular frequency $g_1 - g_2$, of period approximately 242 years (Table 5).

There is an increasing difference with time between the present model taking into account for mutual gravitational interactions between planets one a first hand, and on a second hand the Keplerian model which does not (Sect. 5.1.2). Extrapolated in 2050, both models should show differences of the order of ±10 m/s. A detection of that difference would thus be feasible in next decades.

5.1.4. Stability analysis

In order to analyze the stability of the Keplerian solution (Table 4), we performed a global frequency analysis (Laskar 1993) in the vicinity of this solution, in the same way as achieved for other planetary systems (see, e.g., Correia et al. 2005, 2009, 2010).

For each planet the system is integrated on a regular 2D mesh of initial conditions, with varying semi-major axis and eccentricity, while the other parameters are retained at their Keplerian values (Table 4). The solution is integrated over 1000 years for each initial condition. There are typically 400 steps for the semi-major axis and 100 for the eccentricity. All the stability analyses below have similar numbers of steps in their meshes. The stability criterion is derived with the frequency analysis of the mean longitude over the two consecutive 500-year intervals of time (Laskar 1990, 1993). As in Correia et al. (2005, 2009, 2010), the chaotic diffusion is measured by the variation of the mean motion in each time interval, n_i and n'_i, given by the index $D = \log(|n_i - n'_i|/n_i)$, where i corresponds to the orbit whose initial conditions are not fixed. For regular, quasi-periodic motions, there are no variations in the mean motion along the trajectory, whereas a variation of the mean motion is the signature of chaotic behavior. The result is reported using a color index in Fig. 13, where the red area represents the strongly chaotic trajectories ($D > -2$ in the present case), and the dark-blue area the extremely stable ones ($D < -4$).

In Fig. 13 we show the wide vicinity of the best fitted solution, the minima of the χ^2 level curves corresponding to the Keplerian parameters (Table 4). We observe the presence of the large 12:5 mean motion resonance, which is particularly unstable. We clearly see that the present system is outside this resonance, in a more stable area at the bottom right side (Fig. 13, *top*) or at the bottom left side (Fig. 13, *bottom*).

From the previous stability analysis, it is clear that the HIP 65407 planetary system listed in Table 4 is stable over Gyr timescale. Nevertheless, we also tested directly this by performing a numerical integration of the orbits over 1 Gyr. We used the symplectic integrator SABAC4 of Laskar & Robutel (2001) with a step size of 0.01 yr, including general relativity corrections. The orbits evolve in a regular way, and remain stable throughout the simulation.

5.1.5. Additional constraints from dynamic

We assume that the dynamics of the two planets is not disturbed much by the presence of an additional low-mass, close-by planet.

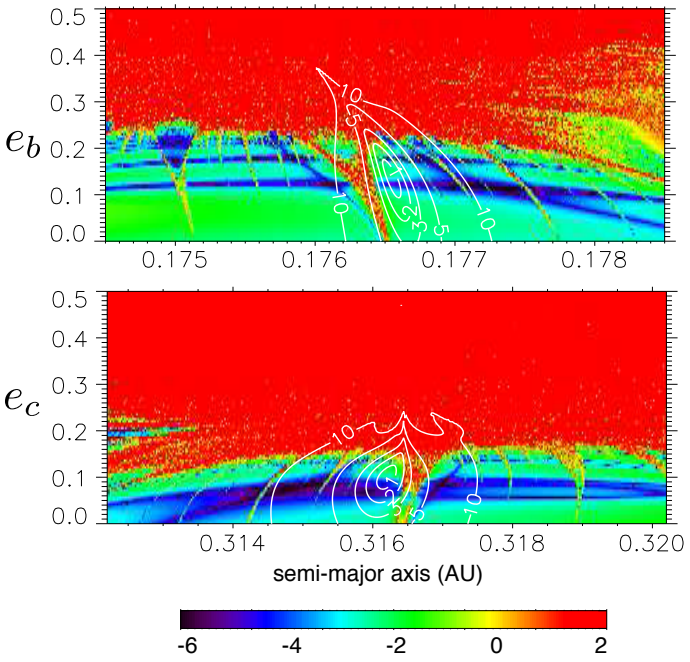

Fig. 13. Stability analysis of the Keplerian fit of the HIP 65407 planetary system. For fixed initial conditions (Table 4), the phase space of the system is explored by varying the semi-major axis a_p and eccentricity e_p of each planet, respectively HIP 65407b and HIP 65407c. The red zone corresponds to highly unstable orbits while the dark-blue region can be assumed to be stable on timescales of a billion years (the color scale shows the D values; see Sect. 5.1.4). The contour curves indicate the 1, 2, 3, 5, 10-σ confidence intervals from $\Delta\chi^2$.

We can thus test the possibility of an additional third planet in the system by varying its semi-major axis, eccentricity, and longitude of the periastron over a wide range, and performing a stability analysis as in Fig. 13. The test was completed for a fixed value $K = 0.1$ m/s, corresponding to a possible Earth-mass planet HIP 65407d at approximately 1 AU, whose radial-velocity amplitude is at the edge of detection. From the analysis of the stable areas in Fig. 14, one can see that additional planets are only possible beyond 0.7 AU, which corresponds to orbital periods longer than 0.6 yr (the orbital period of Venus).

We can also try to find constraints on the maximal masses of the current two-planet system if we assume co-planarity of the orbits. Indeed, up to now we have been assuming that the inclination of the system to the line-of-sight is 90°, which gives minimum values for the planetary masses (Table 4). By decreasing the inclination of the orbital plane of the system, we increase the values of the mass of all planets and repeated a stability analysis of the orbits, like in Fig. 13. As we decrease the inclination, the stable dark-blue areas become narrower, to a point that the minimum χ^2 of the best fit solution lies outside the stable zones. At that point, we conclude that the system cannot be stable anymore. It is not straightforward to find a transition inclination between the two regimes, but we can infer from our plots that stability of the whole system is still possible for an inclination as low as 10°, but becomes impossible for an inclination around 7°. Therefore, we conclude that the maximum masses of the planets may be most probably computed for an inclination around 10°, corresponding to a scaling factor of about 6 to 8 for the possible masses. This corresponds to maximum masses 3.4 M_{Jup} and 6.2 M_{Jup} for HIP 109600b and HIP 109600c, respectively.

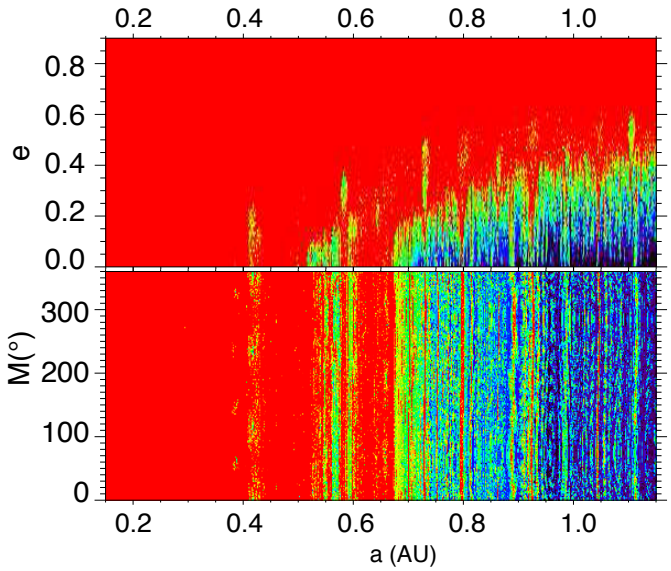

Fig. 14. Possible location of an additional third planet in the HIP 65407 system. The stability of an Earth-mass planet is analyzed, for various semi-major axis versus eccentricity (*top*), or mean anomaly (*bottom*). All the angles of the putative planet are set to 0° (except the mean anomaly in the bottom panel), and in the bottom panel its eccentricity is 0. As in Fig. 13, the color scale corresponds to D values between −6 and 2. The only stable zones where additional planets can be found are the dark-blue regions.

5.2. HD 141399

5.2.1. Keplerian fits

We started observing the low-activity star HD 141399 (BD +47°2267, HIP 77301) with SOPHIE in March 2008. Two inner planets HD 141399b and HD 141399c appeared near resonance 2:1 at periods around 94 and 202 days. We continued the follow-up of that interesting system with SOPHIE+ starting in July 2011. The improved accuracy of SOPHIE+ allow the third planet HD 141399d to be detected at period near 1070 days. We were following up HD 141399 to characterize the additional drift due to a possible fourth, external planet when Voigt et al. (2014) announced their independent detection of a four-planet system around that star based on HIRES and APF data.

Voigt et al. (2014) provided stellar mass and activity index in agreement with what we obtained. We however derived a slightly hotter $T_{\rm eff}$ and a more accurate metallicity. The SOPHIE radial velocities and their four-planet Keplerian model are plotted in Fig. 2 as a function of time. The four phase-folded curves are presented in Fig. 15. The 139 SOPHIE and SOPHIE+ measurements cover seven years of time span and have a relative shift of 25.9 ± 5.8 m/s. Their dispersions around the four-planet Keplerian fit are 12.8 and 4.8 m/s respectively. By comparison, the 77 HIRES measurements from Voigt et al. (2014) cover ten years with a better dispersion around the Keplerian fit of 2.3 m/s, whereas their 14 APF measurements cover half a year with a similar accuracy (2.6 m/s). The four-planet Keplerian fit of our data present a solution similar to the one presented by Voigt et al. (2014). Our periodograms are similar to those they present in their Fig. 4. The peaks in the SOPHIE data are slightly

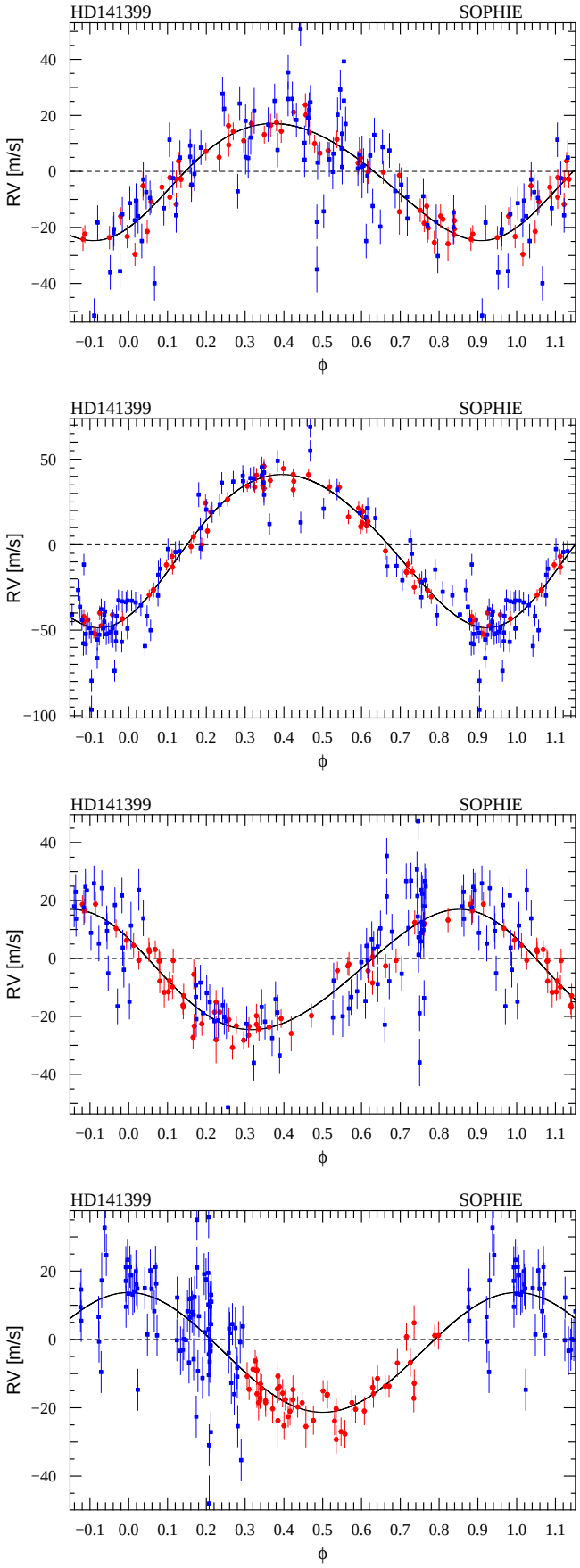

Fig. 15. Phase-folded radial velocity curves for each of the four planets around HD 141399 (planets b, c, d, and e from top to bottom) after removing the effect of the three other planets. The SOPHIE data obtained before/after the June-2011 upgrade are plotted in blue/red with 1-σ error bars, and the Keplerian fits are the solid lines. Orbital parameters corresponding to the fits are reported in Table 4.

stronger and narrower because of our higher number of measurements allowing an improved phase sampling.

The parameters we present in Table 4 are those obtained from the four-planet Keplerian fit of the whole available dataset, i.e. including our new data as well as those of Voigt et al. (2014). The parameters are similar to those reported by Voigt et al. (2014), with some improvements in the uncertainties thanks to the additional data. So we confirm the four-planet system around HD 141399 as presented by Voigt et al. (2014). We note that with its period of 202 days, the insolation level received by HD 141399b is 1.3 ± 0.3 that received by the Earth; the giant planet HD 141399b is thus located in the habitable zone of its host star. The transit probabilities for HD 141399b and HD 141399c are around 1 % but did not attempt any transit detection up to now. The transit probability of the two outer planets is one order of magnitude smaller.

No astrometric motions corresponding to the four planets were detected in the Hipparcos data (Sect. 4), in agreement with the non-detection of any secondary peak in the CCFs. The derived upper limits $M_{\mathrm{p\,max}}$ on the masses of the inner planets b and c are 0.22 and 0.12 $M_\odot$, respectively. No upper limit could be derived for the outer planet e, the time span of the Hipparcos data covering only a small portion of the orbit. In the case of HD 141399d, the Hipparcos data cover slightly more than an orbital period (about three years) and the derived upper limit is 0.04 $M_\odot$; we can thus conclude this companion is clearly substellar, with a true mass below 40 M_{Jup}.

The main issue of discussion is the characterization of the outer planet, HD 141399e, which is a Jupiter near-twin. Its eccentricity and orbital period remain poorly constrained. Even if a complete revolution could have been covered thanks to our new data, similar radial-velocity amplitudes can be produced by simultaneously increasing the eccentricity and the orbital period (as $K^{-1} \propto P^{1/3}\sqrt{1-e^2}$). Voigt et al. (2014) announced a period of 3717 ± 555 days whereas our new data alone provide 3000^{+1300}_{-120} days. Fitting the whole data set provides us the conservative estimation of 5000^{+560}_{-2000} days. We obtained an eccentricity of 0.26 ± 0.22 by the simultaneous fit of the whole dataset, so we can not significantly conclude from the Keplerian fits whether the orbit is circular or not. Voigt et al. (2014) assumed a circular orbit for HD 141399e due to the lack of constraint, acknowledging their are no reasons for this long-period orbit to be perfectly circular.

Following these Keplerian approaches, we made studies of the gravitational interactions between planets, in particular to try to put constraints on the period and eccentricity of the outer planet HD 141399e.

5.2.2. Stability analysis

The solution corresponding to the Keplerian fit (Table 4) allows high values for the eccentricity of the outer planet HD 141399e (e_e = 0.26 ± 0.22). We can test the reliability of this solution by performing a global stability study in its vicinity as explained above for the HIP 65407 system (Sect. 5.1.4). Figure 16 shows the wide vicinity of the best fitted solution. For fixed initial conditions, the phase space of the system is explored here again by varying the semi-major axis a_e and eccentricity e_e. For each initial condition, the system is integrated over 1000 years and the stability criterion is derived with the frequency analysis of the mean longitude. We observe that the minima of the χ^2 level curves corresponding to the Keplerian parameters (Table 4) lies deep inside an extremely chaotic region, so we can conclude that the Keplerian solution is highly unstable.

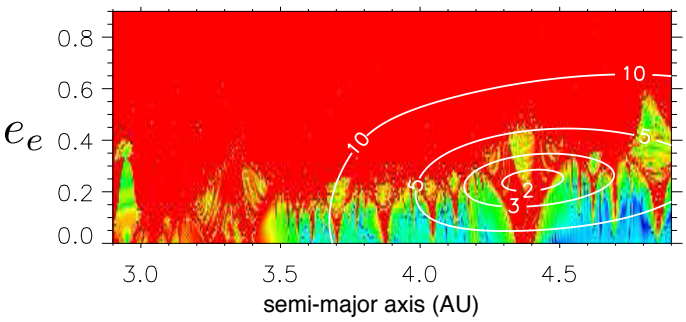

Fig. 16. Stability analysis of the outermost planet HD 141399e for the Keplerian fit (Table 4). For fixed initial conditions, the phase space of the system is explored by varying the semi-major axis a_e and the eccentricity e_e. As in Fig. 13, the color scale shows D values between −6 and 2. The red zone corresponds to highly unstable orbits while the dark-blue region can be assumed to be stable on a billion-years timescale. The contour curves indicate the 2, 3, 5, 10-σ confidence intervals from $\Delta\chi^2$. The best fit lies well inside a red chaotic region.

In Fig. 16 we also observe that any solution with eccentricity above 0.1 is unstable. Therefore, stable solutions for the HD 141399 system require a small eccentricity value for the outermost planet. For simplicity, we proceed as in Vogt et al. (2014) and fix the eccentricity at zero (e_e = 0). We refit the observational data holding this parameter constant, which provides a new orbital configuration for the system. The orbits of the three inner planets are almost unchanged with respect to the Keplerian solution, but the orbital period of the outermost planet is now better constrained. In order to check the robustness of this new solution, we then redo a stability study in the vicinity of the outermost planet. Again, the minima of the χ^2 level curves lie inside a chaotic region, namely, the resonant island corresponding to a 3:1 mean motion resonance between planets HD 141399d and HD 141399e.

Contrarily to other planetary systems (see, e.g., Laskar & Correia 2009), the 3:1 mean motion resonances is unstable in this case. However, just outside this resonance the system appears to be stable. It is then likely that the period ratio between the two outermost planets is slightly shorter or longer than the 3:1 ratio, longer periods being even more stable.

We can test this new scenario by additionally fixing the orbital period of the outer planet slightly above the resonant ratio (we chose P_e = 3412 days here). We fitted the radial velocities holding this parameter constant (together with e_e = 0), which provides a new orbital configuration for the system. The parameters are all similar to the Keplerian ones presented in Table 4, except the period and eccentricity of HD 141399e. Both solutions provide similar fits in terms of dispersion of their residuals, but the new solution is stable whereas the Keplerian one is not. We perform a global stability study in the vicinity of this new solution, which is shown in Fig. 17. We verify that the minima of the χ^2 level curves lie inside stable regions for all four planets in the system. At e_e = 0, the intersection between χ^2 level curves and stabilities zones provides the two intervals corresponding to a_e = 4.33 ± 0.02 and a_e = 4.50 ± 0.08 for HD 141399e, below and above the 3:1 resonance respectively. We finally adopt the solution above the resonance, which is the most stable; it corresponds to the orbital period P_e = 3370 ± 90 days.

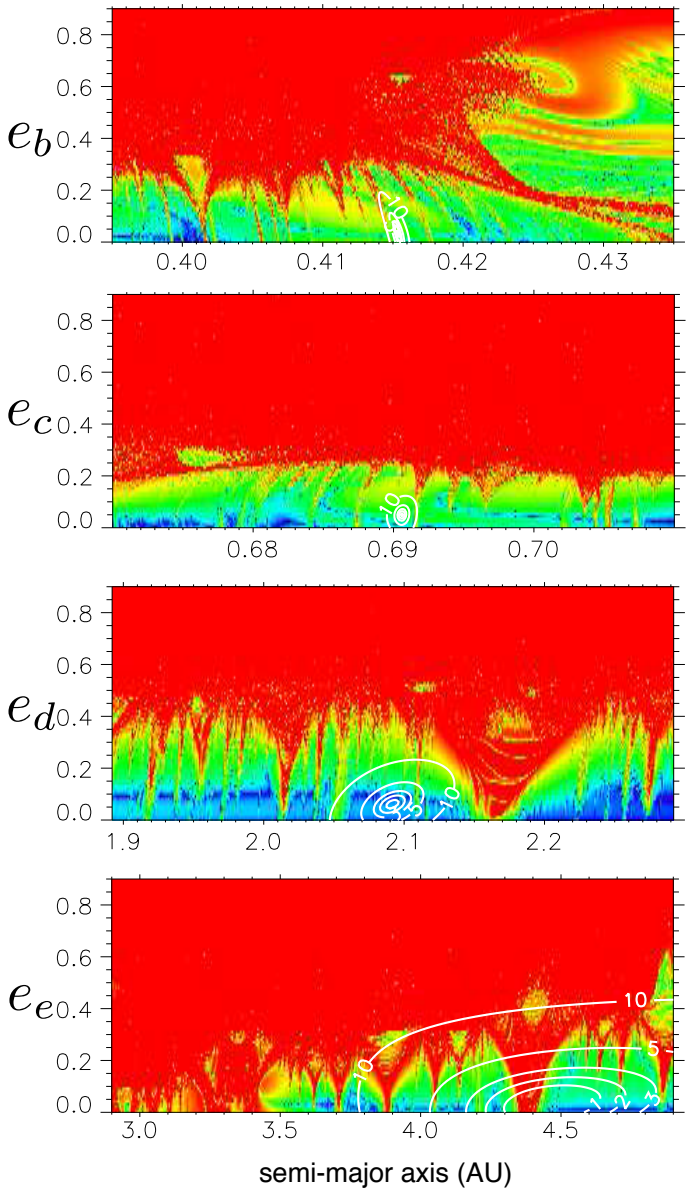

Fig. 17. Stability analysis of the dynamically stable orbital solution for the HD 141399 planetary system (planets HD 141399b, c, d, and e from top to bottom). As in Fig. 13, the color scale shows D values between −6 and 2. The red zone corresponds to highly unstable orbits while the dark-blue region can be assumed to be stable on a billion-years timescale. The contour curves indicate the 1, 2, 3, 5, 10-σ confidence intervals from $\Delta\chi^2$. The minima always lie in a stable region for all four planets in the system.

5.2.3. Additional constraints from dynamic

Similarly to the HIP 65407 system (Sect. 5.1.5), we can assume that the dynamics of the already known planets is not disturbed much by the presence of an additional fifth, low-mass still undetected planet. This test is again completed for a fixed value $K = 0.1$ m/s, corresponding to a possible Earth-mass object at approximately 1 AU, whose radial-velocity amplitude is at the edge of detection. From the analysis of the stable areas in Fig. 18, one can see that additional planets are possible beyond 6 AU, which corresponds to orbital periods longer than 14 years. We also spot some small stability islands at the same semi-major axes of planets HD 141399d and HD 141399e; they correspond to the Lagrange co-orbital resonance of both planets, i.e. Trojan planets.

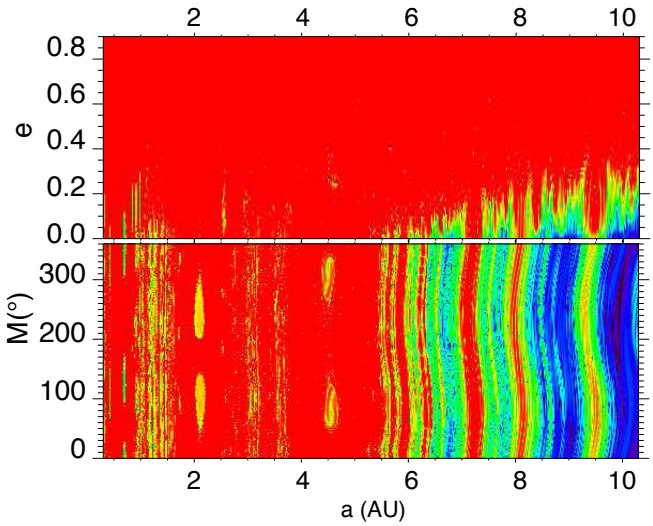

Fig. 18. Possible location of an additional fifth planet in the HD 141399 system. The stability of an Earth-mass planet is analyzed, for various semi-major axis versus eccentricity (*top*), or mean anomaly (*bottom*). All the angles of the putative planet are set to 0° (except the mean anomaly in the bottom panel), and in the bottom panel its eccentricity is 0. As in Fig. 13, the color scale corresponds to D values between −6 and 2. The stable zones where additional planets can be found are the dark-blue regions.

We can also try to find constraints on the maximal masses of the current system if we assume co-planarity of the orbits, as we did above in the case of BD+492211 (Sect. 5.1.5). We conclude that the maximum masses of the planets may be most probably computed for an inclination around 10°, corresponding to 4, 11, 9, and 5 M_{Jup} for planet HD 141399b, c, d, and e, respectively.

6. Conclusions

We have presented new radial velocity measurements of eight stars secured with the spectrograph SOPHIE at the 193-cm telescope of the Haute-Provence Observatory allowing the detection and characterization of new giant extrasolar planets. Seven of the stars allowed us to discover and characterize six new single planets as well as a system including two planets. The eighth star was already known to host a multi-planetary system and we published here our independent measurements and discovery. The 12 giant planets studied here are compared in Fig. 19 with the other known giant exoplanets. We measured their masses with an accuracy of the order of ±5 %. They allow the diversity of extrasolar planets populations to be explored, putting constraints on models of planetary systems formation and evolution.

We summarize below some of their notable properties:

- HD 143105 is one of the brightest stars known to host a hot Jupiter, which could allow numerous follow-up studies to be conducted despite this is not a transiting system;
- HIP 109600b, HD 35759b, HIP 109384b, HD 12484b are new giant, single planets with orbital periods of several months, with no hints of additional companions in the systems;

- the data of the new single-planet systems allow us to exclude the possibility that they actually are composed of two circular planets in 2:1 resonance;
- HD 220842 hosts a massive, giant planet, as well as another substellar companion which need long-term follow-up to be characterized;
- the hot Jupiter HD 143105b and the warm Jupiter HD 12484b are among the few planets detected around moderately fast rotating stars, HD 12484 being in addition a particularly active star;
- the two multi-planetary systems around HIP 65407 and HD 141399 have host stars with particularly high metallicities;
- HIP 109600, HIP 109384, and HD 220842 are metal-poor stars, which is unusual for hosts of giant planets;
- the system around HIP 65407 includes two planets just outside the instable 12:5 resonance, both precessing with a period of 206 years;
- in order to be stable, the nearly Jupiter-twin HD 141399e should have an eccentricity below 0.1 and an orbital period $P = 3370 \pm 90$ days;
- the giant planets HIP 109600b, HIP 109384b, and HD 141399c are located in the habitable zone of their host star, making particularly interesting any potential satellite orbiting these planets, even if such moons remain now out of reach of standard detection technics.

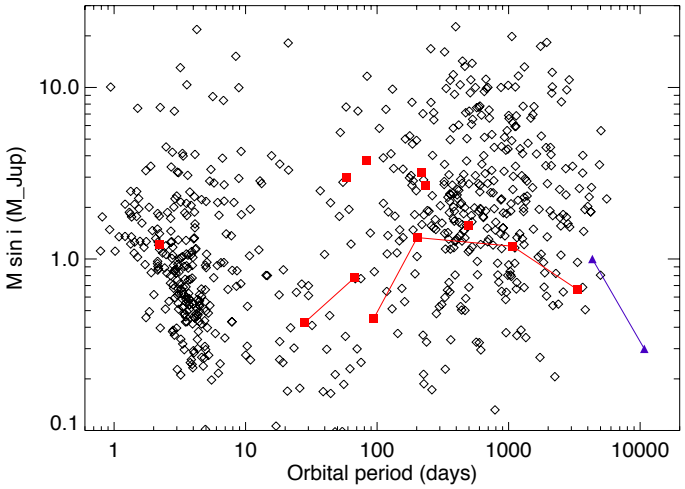

Fig. 19. Sky-project masses and orbital periods of known giant planets (diamonds, from exoplanets.org). The 12 planets from the present study are plotted in red squares. The planets from the multiple systems HIP 65407 and HD 141399 are linked by lines. Jupiter and Saturn are also plotted and linked (blue triangles). With the adopted range in *y*-axes the plot only shows giant planets; planets with sky-projected masses below $0.1\,M_{Jup} = 32\,M_{Earth}$ are not displayed here.

Acknowledgements. We thank all the staff of Haute-Provence Observatory for their support at the 1.93-m telescope and on SOPHIE. This work is also based in part on data collected at Subaru Telescope, which is operated by the National Astronomical Observatory of Japan, and on observations taken with the Remote Observatory Theoretical Astrophysics Tuebingen (ROTAT) located at OHP (France). ROTAT is operated by the Foundation Interactive Astronomy and Astrophysics (Stiftung Interaktive Astronomie und Astrophysik; www.stiftung-astronomie.de). This work was granted access to the HPC resources of MesoPSL financed by the Region Île-de-France and the project Equip@Meso (reference ANR-10-EQPX-29-01) of the programme *Investissements d'Avenir* supervised by the Agence Nationale pour la Recherche. This work was also supported by the "Programme National de Planétologie" (PNP) of CNRS/INSU, the Swiss National Science Foundation, the French National Research Agency (ANR-12-BS05-0012), and the Fundação para a Ciência e a Tecnologia (FCT) through the research grants UID/FIS/04434/2013 and PTDC/FIS-AST/1526/2014. N. C. S. acknowledges support from FCT through Investigador FCT contracts of reference IF/00169/2012, and POPH/FSE (EC) by FEDER funding through the program "Programa Operacional de Factores de Competitividade - COMPETE". A. S. is supported by the European Union under a Marie Curie Intra-European Fellowship for Career Development with reference FP7-PEOPLE-2013-IEF, number 627202. J. H. is supported by the Swiss National Science Foundation (SNSF). A. C. M. C. and J. L. acknowledge support from the "conseil scientifique" of the Observatory of Paris and CIDMA strategic project UID/MAT/04106/2013. P. A. W acknowledges the support of the French Agence Nationale de la Recherche (ANR), under program ANR-12-BS05-0012 "Exo-Atmos".

References

Allard, F., 2014, IAUS, 299, 271
Anderson, D. R., Collier Cameron, A., Delrez, L., et al. 2014, MNRAS, 445, 1114
Anglada-Escudé, G., López-Morales, M., Chambers, J. E. 2010, ApJ, 709, 168
Baraffe, I., Chabrier, G., Fortney, J., Sotin, C. 2014, Protostars and Planets VI, 763
Baranne, A., Queloz, D., Mayor, M., et al. 1994, A&AS, 119, 373
Boisse, I., Moutou, C., Vidal-Madjar, A., et al. 2009, A&A, 495, 959
Boisse, I., Eggenberger, A., Santos, N. C., et al. 2010, A&A, 523, A88
Bonomo, A. S., Santerne, A., Alonso, R., et al. 2010, A&A, 520, A65
Boss, A. P. 2011, ApJ, 731, 74
Bouchy, F., Pont, F., Melo, C., et al., 2005a, A&A, 431, 1105
Bouchy, F., Udry, S., Mayor, M., et al. 2005b, A&A, 444, L15
Bouchy, F., Hébrard, G., Udry, S., et al. 2009, A&A, 505, 853
Bouchy, F., Díaz, R. F., Hébrard, G., et al. 2013, A&A, 549, A49
Bouchy, F., Ségransa, D., Díaz, R. F., et al. 2016, A&A, 585, A46
Brogi, M., Snellen, I. A. G., de Kok, R. J., et al. 2012, Nature, 486, 502
Butler, R. P., Marcy, G. W., Williams, E., et al. 1997, ApJ, 474, L115
Cai, K., Pickett, M. K., Durisen, R. H., Milne, A. M. 2010, ApJ, 716, L176
Carolo, E., Desidera, S., Gratton, R., et al. 2014, A&A, 567, A48
Charbonneau, D., Noyes, R. W., Korzennik, S. G., et al. 1999, ApJ, 522, L145
Charbonneau, D., Brown, T. M., Latham, D. W., Mayor, M. 2000, ApJ, 529, L45
Carter-Bond, J. C., O'Brien, D. P., Raymond, S. N. 2012, ApJ, 760, 44
Chauvin, G., Vigan, A., Bonnefoy, M., et al. 2015, A&A, 573, A127
Chib, S., Jeliazkov, I. 2011, Journal of the American Statistical Association, 453, 270
Correia, A. C. M., Udry, S., Mayor, M., et al. 2005, A&A, 440, 751
Correia, A. C. M., Udry, S., Mayor, M., et al. 2009, A&A, 496, 521
Correia, A. C. M., Couetdic, J., Laskar, J., et al. 2010, A&A, 511, A21
Courcol, B., Bouchy, F., Pepe, F., et al. 2015, A&A, 581, A38
Da Silva, R., Udry, S., Bouchy, F., et al. 2008, A&A, 473, 323
Delisle, J.-B., Laskar, J. 2014, A&A, 570, L7
Díaz, R. F., Santerne, A., Sahlmann, J., et al. 2012, A&A, 538, A113
Díaz, R. F., Rey, J., Demangeon, O., et al. 2016a, A&A, submitted
Díaz, R. F., Ségransan, D., Udry, S., et al., 2016b, A&A, 585, A134
Ehrenreich, D., Bourrier, V., Bonfils, X., et al. 2012, A&A, 547, A18
Fares, R., Donati, J., Moutou, C., et al. 2009, MNRAS, 398, 1383
Gaulme, P., Vannier, M., Guillot, T., et al. 2010, A&A, 518, L153
Guilera, O. M., Brunini, A., Benvenuto, O. G. 2010, A&A, 521, A50
Hagelberg, J., Ségransan, D., Udry, S., Wildi, F. 2016, MNRAS, 455, 2178
Han, E., Wang, S. X., Wright, J. T., et al. 2014, PASP, 126, 827
Hébrard, G., Bonfils, X., Ségransan, D., et al. 2009, A&A, 513, A69
Hébrard, G., Ehrenreich, D., Bouchy, F., et al. 2011, A&A, 527, L11
Hébrard, G., Collier Cameron, A., Brown, D. J. A., et al. 2013, A&A, 549, A134
Heng, K., Demory, B.-O. 2013, ApJ, 777, 100
Jovanovic, N., Martinache, F., Guyon, O., et al. 2015, PASP, 127, 890
Jenkins, J. M., Twicken, J. D., Batalha, N. M., et al. 2015, AJ, 150, 56
Kopparapu, R. K., Ramirez, R., Kasting, J. F., et al. 2013, ApJ, 765, 131
Kürster, M., Trifonov, T., Reffert, S., et al. 2015, A&A, 577, A.103
Laskar, J. 1990, Icarus, 88, 266
Laskar, J. 1993, Physica D Nonlinear Phenomena, 67, 257
Laskar, J., Robutel, P. 2001, Celestial mechanics and dynamical astronomy, 80, 39
Laskar, J., Correia, A. C. M. 2009, A&A, 496, L5
Leigh, C., Collier Cameron, A., Udry, S., et al. 2003, MNRAS, 346, L16
Levison, H. F., Morbidelli, A., Gomes, R.,et al. 2006, Protostars and Planets VI, 669
Lin, D. N. C., Bodenheimer, P., Richardson, D. C., Nature, 380, 606
Lissauer, J. J., Ragozzine, D., Fabrycky, D. C., et al. 2011, ApJS, 197, 8
Liu, S.-F., Agnor, C. B., Lin, D. N. C., Li, S.-L. 2015, MNRAS, 446, 1685
Lovis, C., Dumusque, X., Santos, N. C., et al. 2011, A&A, submitted, arXiv:1107.5325

Madhusudhan, N., Burrows, A. 2012, ApJ, 747, 25
Mamajek, E. E., Hillenbrand, L. A. 2008, ApJ, 687, 1264
Martins, J. H. C., Figueira, P., Santos, N. C., Lovis, C. 2013, MNRAS, 436, 1215
Martins, J. H. C., Santos, N. C., Figueira, P., et al. 2015, A&A, 576, A134
Mayor, M., Queloz, D. 1995, Nature, 378, 355
Mayor, M., Marmier, M., Lovis, C., et al., 2011, A&A, submitted, arXiv:1109.2497
Mordasini, C., Alibert, Y., Benz, W. 2009, A&A, 501, 1139
Moutou, C., Mayor, M., Lo Curto, G., et al. 2011, A&A, 527, A63
Moutou, C., Hébrard, G., Bouchy, F., et al. 2014, A&A, 563, A22
Naef, D., Mayor, M., Pepe, F., et al. 2001, A&A, 375, 205
Noyes, R. W., Hartmann, L. W., Baliunas, S. L., et al. 1984, ApJ, 279, 763
Pepe, F., Mayor, M., Galland, F., et al. 2002, A&A, 388, 632
Perrakis, K., Ntzoufras, I., Tsionas, E. G. 2014, Computational Statistics & Data Analysis, 0, 54
Perruchot, S., Kohler, D., Bouchy, F., et al., 2008, SPIE, 7014, 70140J
Perryman, M. A. C., Lindegren, L., Kovalevsky, J., et al. 1997, A&A, 323, L49
Queloz, D., Henry, G. W., Sivan, J. P., et al. 2001, A&A, 379, 279
Sahlmann, J., Ségransan, D., Queloz, D., et al. 2011, A&A, 525, A95
Sahlmann, J., Fekel, F. C. 2013, A&A, 556, A145
Santos, N. C., Mayor, M., Naef, D., et al. 2000a, A&A, 356, 599
Santos, N. C., Mayor, M., Naef, D., et al. 2000b, A&A, 361, 265
Santos, N. C., Israelian, G., Mayor, M. 2004, A&A, 415, 1153
Santos, N. C., Israelian, G., Mayor, M., et al. 2005, A&A, 437, 1127
Santos, N. C., Udry, S., Bouchy, F., et al. 2008, A&A, 487, 369
Santos, N. C., Sousa, S. G., Mortier, A., et al. 2013, A&A, 556, A150
Sato, B., Fischer, D. A., Henry, G. W., et al. 2005, ApJ, 633, 465
Seager, S., Whitney, B. A., Sasselov, D. D. 2000, ApJ, 540, 504
Ségransan, D., Mayor, M., Udry, S., et al. 2011, A&A, 535, A54
Showman, A. P., Guillot, T. 2002, A&A, 385, 166
Sing, D. K., Fortney, J. J., Nikolov, N., et al. 2016, Nature, 529, 59
Snellen, I. A. G., Brandl, B. R., de Kok, R. J., et al. 2014, Nature, 509, 63
Sousa, S. G., Santos, N. C., Mayor, M., et al. 2008, A&A, 487, 373
Sozzetti, A., Udry, S., Zucker, S., et al. 2006, A&A, 449, 417
Torres, G., Andersen, J., Giménez, A. 2010, A&A Rev., 18, 67
Vogt, S. S., Butler, R. P., Marcy, G. W., et al. 2005, ApJ, 632, 638
Vogt, S. S., Butler, R. P., Rivera, E. J., et al. 2014, ApJ, 787, 97
Wilson, P. A., Hébrard, G., Santos, N. C., et al. 2016, A&A, in press, arXiv:1602.02749
Wittenmyer, R. A., Wang, S., Horner, J., et al. 2013, ApJS, 208, 2
Wright, J. T., Marcy, G. W., Butler, R. P., et al. 2008, ApJ, 683, L63